Endothelial HIF-2α regulates murine pathological angiogenesis and revascularization processes

Nicolas Skuli,[1,2] Amar J. Majmundar,[2,3] Bryan L. Krock,[2] Rickson C. Mesquita,[4] Lijoy K. Mathew,[1,2] Zachary L. Quinn,[1,2] Anja Runge,[1,2] Liping Liu,[1,2] Meeri N. Kim,[4] Jiaming Liang,[4] Steven Schenkel,[4] Arjun G. Yodh,[4] Brian Keith,[1,5] and M. Celeste Simon[1,2,6]

[1]Howard Hughes Medical Institute, [2]Abramson Family Cancer Research Institute, [3]School of Medicine, [4]Department of Physics and Astronomy, [5]Department of Cancer Biology, and [6]Department of Cell and Developmental Biology, University of Pennsylvania, Philadelphia, Pennsylvania, USA.

Localized tissue hypoxia is a consequence of vascular compromise or rapid cellular proliferation and is a potent inducer of compensatory angiogenesis. The oxygen-responsive transcriptional regulator hypoxia-inducible factor 2α (HIF-2α) is highly expressed in vascular ECs and, along with HIF-1α, activates expression of target genes whose products modulate vascular functions and angiogenesis. However, the mechanisms by which HIF-2α regulates EC function and tissue perfusion under physiological and pathological conditions are poorly understood. Using mice in which *Hif2a* was specifically deleted in ECs, we demonstrate here that HIF-2α expression is required for angiogenic responses during hindlimb ischemia and for the growth of autochthonous skin tumors. EC-specific *Hif2a* deletion resulted in increased vessel formation in both models; however, these vessels failed to undergo proper arteriogenesis, resulting in poor perfusion. Analysis of cultured HIF-2α–deficient ECs revealed cell-autonomous increases in migration, invasion, and morphogenetic activity, which correlated with HIF-2α–dependent expression of specific angiogenic factors, including delta-like ligand 4 (Dll4), a Notch ligand, and angiopoietin 2. By stimulating Dll4 signaling in cultured ECs or restoring Dll4 expression in ischemic muscle tissue, we rescued most of the HIF-2α–dependent EC phenotypes in vitro and in vivo, emphasizing the critical role of Dll4/Notch signaling as a downstream target of HIF-2α in ECs. These results indicate that HIF-1α and HIF-2α fulfill complementary, but largely nonoverlapping, essential functions in pathophysiological angiogenesis.

Introduction

The therapeutic manipulation of angiogenesis holds great promise for treating diverse pathological conditions, including cancer, macular degeneration, atherosclerosis, and peripheral arterial disease (PAD) (1, 2). However, the ability to reliably inhibit (or promote) angiogenesis in clinical settings requires a thorough appreciation of the complex molecular events that coordinate vessel sprouting and remodeling (3, 4). These processes are clearly influenced by reductions in local O_2 concentration (hypoxia), which can arise as a consequence of ischemic insult or rapid cell division during solid tumor growth (5, 6). Elucidating the mechanisms by which hypoxic stress modulates the activity of vascular ECs is therefore critical to our understanding of disease-associated angiogenesis.

Cells respond to hypoxic stress through multiple mechanisms, including the stabilization of hypoxia-inducible factors (HIFs), which directly regulate the expression of more than 150 target genes that modulate angiogenesis, cell metabolism, proliferation, survival, and migration (reviewed in ref. 6). Mammalian HIFs function as heterodimers composed of either HIF-1α (7) or HIF-2α (8) bound to HIF-1β (also known as aryl hydrocarbon nuclear translocator). HIF-1α appears to be ubiquitously expressed, whereas HIF-2α is detected in a more restricted set of cell types, including vascular ECs, hepatocytes, type II pneumocytes, and macrophages. A third mammalian HIF-α subunit, HIF-3α (9), has also been described, although its role in hypoxic responses is less well understood.

HIF activity is controlled by hypoxia-induced posttranslational stabilization of HIF-α subunits, which are otherwise hydroxylated, ubiquitylated, and degraded under normoxic conditions through the activity of HIF-specific prolyl hydroxylases (PHD1–PHD3) and other enzymes (6, 10). Additionally, oncogenic signaling pathways have been reported to influence HIF-α levels, in part by regulating the rate of HIF-α protein translation. Although HIF-1α and HIF-2α share highly conserved structural features, oxygen-mediated stabilization, and numerous target genes, mounting evidence indicates that each protein has remarkably distinct functions in specific cellular contexts. These differences are mediated in part by regulation of unique target genes, but also by opposing influences on other critical factors, including c-Myc (11), p53 (12), and nitric oxide (13).

Emerging evidence suggests that HIF-1α and HIF-2α have important and independent effects on pathological angiogenesis. For example, femoral artery ligation (FAL) experiments revealed decreased limb perfusion and increased spontaneous amputation in heterozygous *Hif1a*$^{+/-}$ mice, or in wild-type mice treated with the HIF-1α inhibitor 2-methoxyestradiol (14). Furthermore, delivery of adenovirus encoding constitutively active HIF-1α stimulated reperfusion following FAL and hindlimb ischemia in older wild-type mice or in diabetic mice (15); in each case, the effects of HIF-1α were attributed to mobilization of circulating angiogenic cells. EC-specific HIF-1α expression is also required for robust tumor angiogenesis, tumor growth, and wound healing by promoting EC proliferation and survival (16). These effects were correlated with HIF-1α–dependent expression of VEGF and other angiogenic factors.

Conflict of interest: The authors have declared that no conflict of interest exists.
Citation for this article: *J Clin Invest.* 2012;122(4):1427–1443. doi:10.1172/JCI57322.

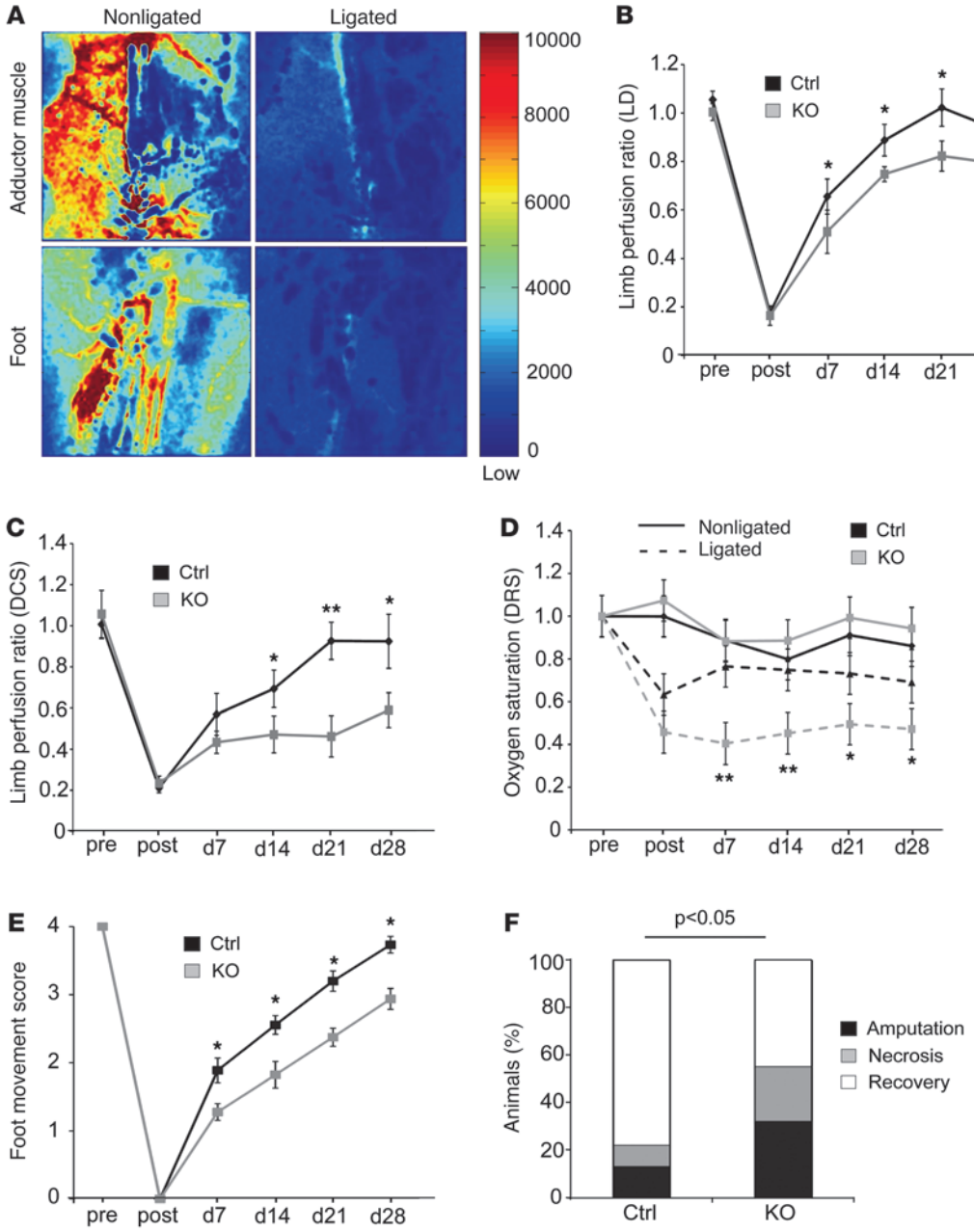

Figure 1

Endothelial HIF-2α deletion affects blood flow, foot movement recovery, and necrosis after femoral artery ligation (FAL). Blood flow, foot movement score, and necrosis were assessed for control and KO mice. Blood flow was quantified by laser Doppler (LD) and diffuse correlation spectroscopy (DCS) before (Pre), immediately after (Post), and on the indicated days following FAL. (**A**) Representative images obtained by Speckle imaging technique showing the efficiency of the surgery distally to the occlusion side. (**B** and **C**) Quantitative LD and DCS analyses showing the left limb/right limb ratio after occlusion of the femoral artery. KO mice displayed delayed restoration in perfusion compared with control mice. (**D**) Oxygen saturation in ligated and nonligated limb was determined for control and KO mice using diffuse reflectance spectroscopy at several time points. (**E**) Foot movement was determined and scored between 0 and 4 as a functional readout parameter to assess flow deficits after ischemia. Active foot movement was significantly impaired in KO mice. (**F**) Percent mice presenting necrosis or amputation. More KO mice had to be euthanized due to amputation or necrosis of the limb. $n = 20$ (control); 22 (KO). $^*P < 0.05$; $^{**}P < 0.01$.

The specific contribution of EC HIF-2α to ischemia-induced angiogenesis has not been investigated directly, despite the fact that HIF-2α is highly expressed in these cells. An indirect role for HIF-2α in ischemic responses has been reported for PHD1-deficient mice subjected to FAL; specifically, muscles in *Phd1*$^{-/-}$ mice are protected from ischemic stress by alterations in glucose metabolism and reactive oxygen species production, phenotypes largely reversed by HIF-2α haplodeficiency (17). In contrast, we previously demonstrated that EC-specific deletion of HIF-2α caused defects in EC adhesion and vessel integrity (18). Moreover, HIF-2α abla-

tion in ECs inhibited subcutaneous xenograft tumor growth and angiogenesis (18, 19), which were associated with greater intratumoral hypoxia and fewer functional vessels relative to tumors grown in control mice. HIF-2α was also implicated as a critical downstream effector modulating normalization of tumor vessels in *Phd2*$^{+/-}$ mice, which correlates with improved tumor oxygenation and decreased metastasis (20).

In the current study, we use critical limb ischemia and autochthonous skin tumor models to directly assess the cellular and molecular mechanisms by which HIF-2α regulates EC function and pathological angiogenesis. Mice with EC-specific HIF-2α deletion produced increased numbers of newly formed vessels in ischemic muscles and autochthonous tumors; however, these vessels failed to remodel effectively, thereby reducing overall vascular area, blood flow, and tissue oxygenation. Purified HIF-2α–deficient ECs displayed increased migration, invasion, and tube formation in vitro as well as reduced hypoxic expression of important angiogenic molecules, including angiopoietin 2 (Ang2) and adrenomedullin (ADM1). Interestingly, similar effects on tumor angiogenesis were observed upon inhibition of the delta-like ligand 4/Notch (Dll4/Notch) pathway (21), and we further demonstrated that HIF-2α specifically regulated hypoxic expression of the Notch ligand Dll4 as well as downstream effectors of the Dll4/Notch pathway, both in vivo and in vitro. Finally, we showed that exogenously supplied Dll4 complemented the phenotypes of HIF-2α–deficient ECs both in vitro and in vivo. Collectively, these data identified EC-specific functions for HIF-2α that we believe to be novel, both in restricting angiogenic sprouting and promoting vascular remodeling, and demonstrated that HIF-1α and HIF-2α have fundamentally distinct, but apparently complementary, EC-specific functions in pathophysiological angiogenesis. Whereas previous reports demonstrated that HIF-1α promotes EC proliferation and VEGF expression, thereby driving new vessel formation (16), HIF-2α was essential for remodeling new vessels into a functional vasculature, partly through Notch pathway regulation. These data support the hypothesis that by promoting apparently antagonistic molecular responses, HIF-1α and HIF-2α expression in ECs modulate angiogenic responses in the context of pathophysiological hypoxia to produce a functional vasculature.

Results

Endothelial HIF-2α deletion disrupts blood flow recovery after FAL. Our previous studies suggested that HIF-2α would be a critical regulator of vascular regeneration and angiogenesis in the context of peripheral vascular disease. To test this hypothesis, we challenged control mice or mice lacking EC-specific HIF-2α expression (referred to herein as KO mice) with FAL and investigated subsequent blood flow, vessel regeneration, and tissue damage. Blood flow in the adductor muscles and feet of control and KO mice was assessed before and after surgery using Speckle imaging techniques, which showed markedly decreased blood flow in the ligated limb (Figure 1A). Perfusion in ligated and nonligated limbs was then measured 7, 14, 21, and 28 days after surgery using laser Doppler flowmetry (LD), which detects blood flow in superficial tissues. In addition, diffuse correlation spectroscopy (DCS) was used to measure oxygenation and metabolic processes of the microvasculature in deeper tissues (22). Both LD and DCS analyses revealed significantly reduced flow characteristics in ligated limbs of control and KO animals after surgery compared with nonligated contralateral limbs (Figure 1, B and C), indicative of comparable levels of postprocedure ischemia in both strains. As expected, a steady recovery of blood flow in the ligated limb was evident beginning 7 days postsurgery; however, blood flow recovery was significantly attenuated in KO versus control mice over the entire observation period (Figure 1, B and C). Moreover, KO mice never fully recovered normal blood flow, even after 28 days, in contrast to control mice.

Similarly, ligated limbs in both KO and control strains displayed equivalent reductions in oxygen saturation immediately postsurgery. Oxygen saturation returned to nearly normal levels in control mice by 7 days postsurgery, whereas blood oxygen saturation remained significantly reduced in KO mice over the 28-day postsurgery observation period (Figure 1D), which indicates that ligated limbs in KO mice remain substantially more ischemic than those in control mice.

The functional consequences of impaired revascularization in KO mice were investigated using a scoring system based on active foot movement (see Methods and ref. 14). Foot movement in the ligated limb was significantly reduced at days 7, 14, 21, and 28 in KO mice compared with control animals (Figure 1E). Finally, KO mice exhibited increased incidence of tissue necrosis and spontaneous amputation compared with control mice (Figure 1F), further suggesting that HIF-2α activity in ECs is required for proper vascular recovery after FAL.

Impaired postnatal arteriogenesis and angiogenesis in mice with EC-specific HIF-2α deletion. To investigate the cellular nature of the perfusion defects observed in ischemic KO muscles, we quantified collateral arterial growth and capillary formation in affected tissues. Prior to surgery, histomorphometry revealed no difference in the size of collateral arteries in contralateral limbs of control and KO mice. By 28 days postsurgery, control mice displayed increased collateral arterial diameter and wall area in affected tissues, consistent with active arterial remodeling and growth; however, this enhancement was significantly diminished in KO mice (Figure 2, A–C). Furthermore, smooth muscle cell recruitment to collateral arteries was also reduced in KO mice compared with controls (Supplemental Figure 1; supplemental material available online with this article; doi:10.1172/JCI57322DS1), revealing a role for EC-specific HIF-2α expression in injury-induced arteriogenesis.

Capillary density was enhanced in ischemic muscles from all mice after 28 days, although ischemic KO muscles displayed a surprising increase in vessel density relative to controls (Figure 2, D and E). Nevertheless, the corresponding total vascular area (rhodamine-lectin–labeled vessels plus lumens) was actually reduced in ischemic KO muscles compared with control muscles (Figure 2F). These data, as well as the relative paucity of capillaries with large lumens in ischemic KO muscles (Figure 2, D and F), suggest that KO vessels have an impaired ability to remodel into fully functional vessels in ischemic tissue. This hypothesis is supported by the observation that muscles from ligated limbs in KO mice exhibited more extensive areas of injury and necrosis than those in control mice (Figure 2, G and H). Serum creatine kinase activity, a marker of muscle damage, was elevated in all mice after FAL; however, KO mice retained persistently higher creatine kinase activity than control mice (Figure 2I), reflecting greater muscle damage in these mice. Collectively, these results strongly suggest that recovery from FAL-induced ischemia requires EC HIF-2α activity; otherwise, incomplete or aberrant arteriogenesis and angiogenesis occur, with consequent increases in tissue damage.

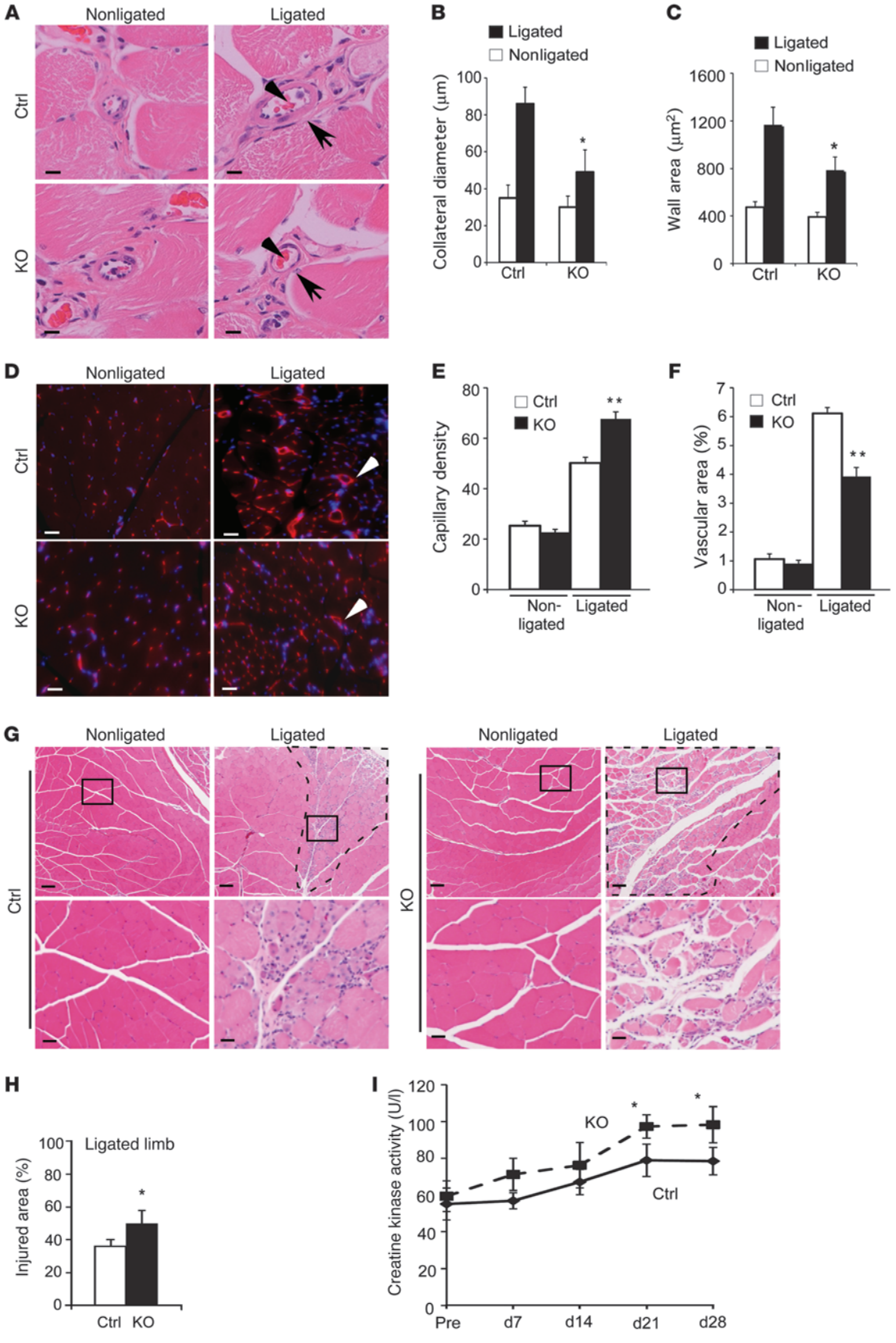
A
Nonligated
Ligated
Ctrl
KO
B
Ligated
Nonligated
Collateral diameter (μm)
100
80
60
40
20
0
*
Ctrl
KO
C
Ligated
Nonligated
Wall area (μm²)
1600
1200
800
400
0
*
Ctrl
KO
D
Nonligated
Ligated
Ctrl
KO
E
Ctrl
KO
Capillary density
80
60
40
20
0
**
Non-ligated
Ligated
F
Ctrl
KO
Vascular area (%)
7
6
5
4
3
2
1
0
**
Non-ligated
Ligated
G
Nonligated
Ligated
Nonligated
Ligated
Ctrl
KO
H
Ligated limb
Injured area (%)
100
80
60
40
20
0
*
Ctrl
KO
I
Creatine kinase activity (U/l)
120
100
80
60
40
20
0
KO
Ctrl
*
*
Pre
d7
d14
d21
d28

Figure 2
Impaired postnatal arteriogenesis and angiogenesis and increased necrosis in KO mice. (**A**) Representative H&E-stained sections of adductor muscle from ligated and nonligated limb in control and KO mice. Arrows indicate collateral wall. Arrowheads indicate collateral lumen. (**B** and **C**) Histomorphometric analysis of collateral lumen and wall area showing deficient collateral artery growth in KO mice. Arrows indicate collateral wall, arrowheads indicate collateral lumen. (**D**–**F**) Rhodamine-lectin staining (**D**) showed increased vessel density (**E**) but decreased vascular area (**F**) in adductor muscle of KO mice. Arrowheads indicate capillaries. (**G**) H&E-stained sections of adductor muscle for ligated and nonligated limb in control and KO mice. Boxed regions are shown at higher magnification below. Dashed outlines denote damaged or injured areas within muscle. (**H**) Percent injured area per section determined for ligated limb. (**I**) Levels of creatine kinase activity assessed in serum after ligation. Scale bars: 20 μm (**A** and **C**); 80 μm (**G**, top); 40 μm (**G**, bottom). Original magnification, ×200 (**A** and **G**, bottom); ×400 (**D**); ×100 (**G**, top). n = 8 (control); 9 (KO). $^*P < 0.05$; $^{**}P < 0.01$.

EC HIF-2α deletion affects tumor growth and vasculature in a skin carcinogenesis model. To determine whether EC-specific HIF-2α expression was required for vessel sprouting and remodeling in a distinct model of neovascularization, we investigated the growth and angiogenesis of carcinogen-induced skin epithelial tumors in KO and control mice. Previous experiments using subcutaneous xenograft tumors indicated that EC-specific HIF-2α deletion inhibited tumor growth (18); however, rapid growth of Lewis lung carcinoma and B16 melanoma xenografts do not always reflect the physiology of bona fide autochthonous tumors. To address this point, skin papillomas were induced in control and KO mice using a standard DMBA/TPA protocol (see Methods) for 25 weeks (Figure 3A). After 5 weeks, epidermal tumors were apparent in all treated mice (Figure 3B), and their number and size increased with time (Figure 3C). Interestingly, no difference in the percentage of mice with small (0–3 mm) and medium (3–6 mm) skin tumors was observed between KO and control mice; however, the formation of large (>6 mm) skin tumors was delayed in KO mice compared with controls (Figure 3C). Large tumors appeared approximately 5 weeks earlier in control mice than in KO mice, and after 20 weeks, control mice were more likely to develop large papillomas than KO mice (4 of 8 control, versus 1 of 8 KO). A similar pattern was observed after 25 weeks: 6 of 8 control mice, compared with 3 of 8 KO mice, presented with large tumors (Figure 3C). Finally, control mice formed 10 times as many large papillomas at 25 weeks (control, 2.23 ± 1.17 papillomas/mouse; KO, 0.23 ± 0.60 papillomas/mouse; $P < 0.05$; Figure 3, D and E).

Immunohistochemical and histological analyses of skin papillomas from KO mice revealed impaired angiogenesis compared with control mice (Figure 3, F–L). Specifically, skin tumors in KO mice were characterized by an increased number of small vessels and a reduced number of large vessels compared with control mice (Figure 3G). Rhodamine-lectin staining confirmed increased functional capillary density and decreased lumen area in KO skin tumors (Figure 3, H–J), similar to results in ischemic muscle. Moreover, immunohistochemical staining for desmin and α–smooth muscle actin (Figure 3K and Supplemental Figure 1) revealed a significant decrease in the degree of mural cell coverage of tumor vessels in KO mice (Figure 3L).

Collectively, our data demonstrated that HIF-2α–deficient ECs produced elevated numbers of capillaries compared with controls in 2 distinct pathophysiological angiogenesis models (ischemic muscle tissue and autochthonous skin tumors). In each case, however, these HIF-2α–deficient capillaries failed to remodel into mature, functional blood vessels, resulting in decreased perfusion.

Cell-autonomous effects of HIF-2α or HIF-1α deletion in ECs. To identify possible cell-autonomous functions of HIF-2α that underlie the angiogenic phenotypes observed in vivo, we generated primary EC cultures from mice carrying a conditional floxed *Hifa* allele and the *Ubc-CreER* transgene (see Methods and refs. 23, 24). Independent cultures of immortalized lung ECs that expressed characteristic cell surface markers (CD31, ICAM2, and vWF) and took up the EC-diagnostic compound DiI-Ac-LDL (Supplemental Figure 2) were isolated. Subsequent deletion of the conditional *Hif2a* allele was induced by tamoxifen treatment, as previously described (18). PCR analysis revealed efficient recombination of the *Hif2a* floxed allele, and Western blot analysis confirmed loss of HIF-2α protein expression in these cells (Supplemental Figure 2). Similar analyses revealed efficient recombination of the conditional *Hif2a* allele in purified EC populations from muscle and skin of KO mice (Supplemental Figure 3 and ref. 25).

Tamoxifen-induced HIF-2α deletion had no statistically significant effect on the proliferation or viability of ECs cultured under normoxic (21% O_2) or hypoxic (0.5% O_2) conditions, compared with matched HIF-2α–expressing EC controls (Supplemental Figure 4, A–F). Similarly, no significant difference in EC proliferation was observed between control and KO ischemic muscle (Supplemental Figure 4, G and H). We next investigated the effects of HIF-2α deletion on EC migration, invasion, and adhesion (Figure 4 and Supplemental Figure 5), which are essential for physiological and pathophysiological angiogenesis. Scratch assays revealed no obvious difference in migration under normoxic conditions for control or KO ECs (Figure 4A); however, EC migration was markedly increased under hypoxic conditions and further elevated by HIF-2α deletion (Figure 4, A and B). Related experiments using Boyden chambers showed that control and KO ECs exhibited enhanced invasive behavior in hypoxia, which was also significantly increased by HIF-2α deletion (Figure 4, C and D). Hypoxic KO ECs also exhibited reduced adhesion to dishes coated with collagen (but not plastic), which correlated with elevated numbers of visible filopodial extensions (Supplemental Figure 5), consistent with increased mobility of these cells.

Finally, we measured the ability of HIF-2α–deficient ECs to form cytoplasmic extensions (also referred to as *cords*) when cultured in Matrigel, an established in vitro angiogenesis assay. Under normoxic conditions, matched control and KO ECs formed cords within 8 hours of plating (Figure 4, E–H). The number and length of EC cords, as well as the number of branch points and internal lumens formed, was enhanced by hypoxic conditions, but again significantly elevated by HIF-2α deletion (Figure 4, F–H). These results surprisingly indicated that HIF-2α normally restrains specific EC processes associated with angiogenesis, including EC migration, invasion, and cord formation in vitro. Our data suggest that the aberrant vascular remodeling observed in ischemic muscles and autochthonous tumors from KO mice may be caused by inappropriate activation of these processes in hypoxic HIF-2α–deficient ECs.

To confirm that our results were specific to HIF-2α deletion, we also generated HIF-1α–deficient immortalized EC cultures (Supplemental Figure 2). In contrast to HIF-2α, and consistent

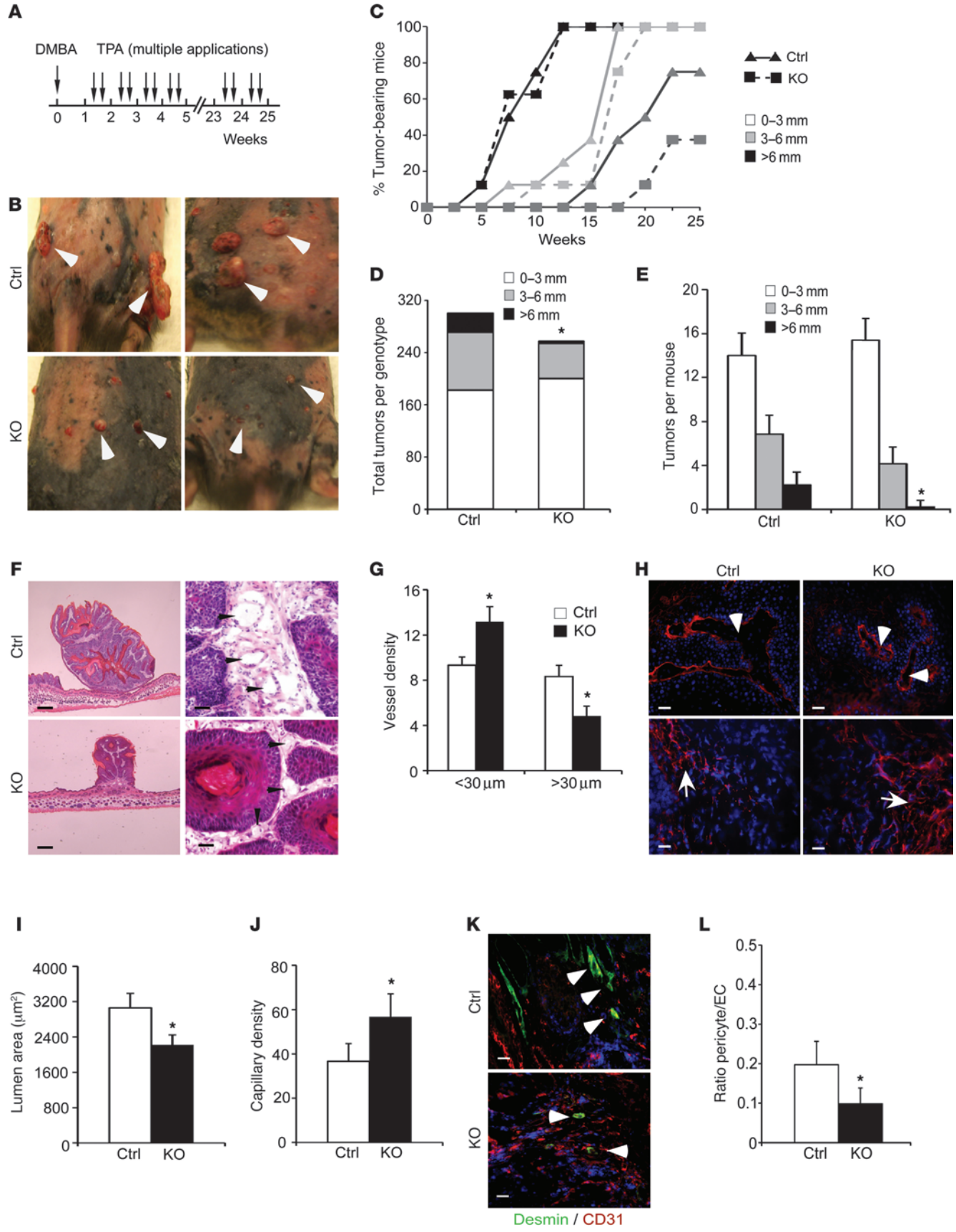
A
DMBA
TPA (multiple applications)
0 1 2 3 4 5 23 24 25
Weeks
B
Ctrl
KO
C
% Tumor-bearing mice
Weeks
Ctrl
KO
0–3 mm
3–6 mm
>6 mm
D
Total tumors per genotype
0–3 mm
3–6 mm
>6 mm
Ctrl
KO
E
Tumors per mouse
0–3 mm
3–6 mm
>6 mm
Ctrl
KO
F
Ctrl
KO
G
Vessel density
Ctrl
KO
<30 μm
>30 μm
H
Ctrl
KO
I
Lumen area (μm²)
Ctrl
KO
J
Capillary density
Ctrl
KO
K
Ctrl
KO
Desmin / CD31
L
Ratio pericyte/EC
Ctrl
KO

Figure 3
Endothelial HIF-2α deletion affects tumor formation and angiogenesis in a DMBA/TPA-induced tumorigenesis model. (**A**) Skin carcinogenesis was induced using the DMBA/TPA protocol for 25 weeks. Lesions with diameters of 0–3 mm, 3–6 mm, and >6 mm were recorded as tumors. (**B**) Representative images of tumor formation on the dorsal skin of control and KO mice after 25 weeks. Tumors of different sizes are shown by arrowheads. (**C**) Incidence of tumor formation, shown as percent mice with 0–3 mm, 3–6 mm, and >6 mm tumors during the 25 weeks of treatment. (**D**) Number of tumors per genotype. (**E**) Number of tumors per mouse. (**F**) Representative H&E-stained sections of skin tumors. Arrowheads denote vessels within tumors. (**G**) Vessel density, determined for vessels <30 μm and >30 μm in diameter. (**H**–**J**) Rhodamine-lectin staining (**H**) showed decreased lumen area (**I**), but increased capillary density (**J**), in skin tumors of KO mice. Arrows indicate capillaries; arrowheads indicate vessel lumens. (**K**) Desmin (pericyte marker) and CD31 (EC marker) costaining in skin tumors from control and KO mice. (**L**) Pericyte recruitment, expressed as the pericyte/EC ratio, was diminished for tumors grown in KO mice. Scale bars: 800 μm (**F**, left); 25 μm (**F**, right); 40 μm (**H**); 20 μm (**K**). Original magnification, ×50 (**F**, left); ×200 (**F**, right); ×400 (**K**). $n = 10$ (control); 11 (KO). *$P < 0.05$.

with a previous report (16), deletion of HIF-1α reduced EC viability and proliferation (Supplemental Figure 6), as well as migration and invasion under hypoxic conditions (Supplemental Figure 7). Moreover, the formation of cords, branch points, and lumens in Matrigel culture was strongly inhibited in HIF-1α–deficient ECs under hypoxia (Supplemental Figure 7). Collectively, these data suggest that HIF-1α and HIF-2α exhibit unique and apparently antagonistic effects on vascular remodeling and angiogenesis.

EC HIF-2α deficiency impairs hypoxic induction of genes regulating angiogenesis and arteriogenesis. Previous data indicate that HIF-2α regulates multiple genes encoding angiogenic factors such as Dll4, ADM1, and Ang2 (18, 26). We hypothesized that altered expression of these genes could account, at least in part, for the vascular phenotypes we observed in KO ECs, both in vitro and in vivo. For example, inhibition of Dll4 signaling has been shown to result in proliferation of disorganized capillaries, leading to decreased tumor perfusion and growth (21). ADM1 also modulates arterial differentiation and vascular development, in part by regulating the Dll4/Notch pathway (27–29). Finally, Ang2 promotes arteriogenesis and tissue reperfusion after artery occlusion (30).

Quantitative real-time RT-PCR (qRT-PCR) analyses confirmed that HIF-2α deletion greatly inhibited the hypoxic induction of *Ang2*, *Dll4*, and *Adm1* mRNA expression in ECs (Figure 5A), although the absolute level of mRNA expression varied among independent EC lines. The hypoxic induction of multiple Notch target genes, including *Hey1*, *Hey2*, and *Hes1*, was also significantly inhibited in HIF-2α–deficient ECs. This response was selective, in that other genes encoding related angiogenic regulators (*Vegf*, *Tie2*, and *Ang1*) were unaffected by HIF-2α deletion. Of note, HIF-1α deletion in ECs had relatively minor effects on hypoxic *Dll4*, *Adm1*, *Ang2*, and Notch target gene induction, but significantly reduced the hypoxic induction of *Vegf* and *Ang1* transcript levels (Figure 5B), in contrast to HIF-2α deletion (18). These data are consistent with the notion that HIF-2α and HIF-1α regulate the expression of distinct angiogenic factors in ECs. Interestingly, deletion of either HIF-1α or HIF-2α reduced the expression of the arterial marker *Ephb2* in ECs, but had no effect on the expression of the venous marker *Ephb4* (Figure 5, A and B).

The differential expression of *Dll4* and *Ang2* were of particular interest, as the primary angiogenic phenotypes in KO mice (specifically, increased nonproductive capillary formation and reduced arteriogenesis) were similar to angiogenic phenotypes resulting from decreased *Dll4* and *Ang2* expression, respectively (30, 31). To determine whether changes in *Dll4* and *Ang2* transcript levels in cultured HIF-2α KO ECs correlated with altered EC protein expression in our in vivo models, we performed immunofluorescence on the ischemic muscle tissues and skin tumors described in Figures 1–4. Previous work demonstrated that *Dll4* transcription is induced in adductor muscles after FAL (31), and whole-mount immunofluorescent analysis revealed similar elevation of Dll4 protein expression in vessels of ischemic muscles in control mice 7 days after FAL (Figure 5C). In contrast, Dll4 expression in KO ischemic muscle was reduced by 30% (Figure 5D).

Ang2 protein expression is also induced in ischemic adductor muscles in response to FAL, where it likely contributes to vessel enlargement and remodeling (30). We assessed circulating Ang2 protein levels in the serum of control and KO mice at multiple time points after FAL. In control mice, serum Ang2 levels increased 3-fold (to 120 ± 16 pg/ml) 7 days postsurgery, and gradually returned to starting levels (39 ± 6 pg/ml) 28 days postsurgery. This increase in serum Ang2 levels was dramatically inhibited in KO mice, reaching a peak of only 63 ± 7 pg/ml 7 days postsurgery and returning to starting levels 14 days postsurgery (Figure 5E). We also determined that Ang2 staining was increased, and localized primarily to larger collateral vessels, in vessels of ischemic muscles from control mice, whereas Ang2 staining intensity was reduced by 56% in ischemic muscles from KO mice (Figure 5, F and G).

Finally, we performed immunofluorescence analysis of Dll4 expression in skin tumors from control and KO mice. Vessels from control tumors exhibited robust Dll4 expression, which was reduced by 40% in tumors from KO mice (Figure 5, H and I). Collectively, these data indicate that Dll4 and Ang2 expression in ECs is regulated by HIF-2α both in vitro and in vivo and that reduced Dll4 and Ang2 expression in KO mice correlates with impaired tissue recovery from ischemia and tumor angiogenesis.

Dll4/Notch pathway inhibition phenocopies HIF-2α deficiency in EC network formation, migration, and adhesion. To investigate the specific role of Dll4/Notch signaling in the HIF-2α–dependent EC phenotypes, we attempted to manipulate the expression of specific Dll4/Notch pathway components in cultured ECs using gene transfer methods; however, these approaches were hampered by low transfection efficiencies (data not shown). We therefore tested whether the γ-secretase inhibitor N-[N-(3,5-difluorophenacetyl-L-alanyl)]-S-phenylglycine t-butyl ester (DAPT), which blocks Notch cleavage and activation (32), could phenocopy HIF-2α deficiency in control ECs. In initial experiments, we verified the efficacy of DAPT treatment by monitoring the accumulation of Notch intracellular domain (NICD) protein, as well as Notch target gene expression (Supplemental Figure 8). Robust induction of NICD protein accumulation in hypoxic control ECs was effectively blocked by DAPT treatment, which also inhibited the more meager NICD induction observed in KO ECs (Supplemental Figure 8A). Corresponding hypoxic induction of the Dll4/Notch pathway target genes *Hes1* and *Hey2* was also significantly impaired in ECs treated with DAPT (Supplemental Figure 8B).

We then investigated the effects of DAPT treatment (and Notch inhibition) on EC migration, invasion, and tube formation assays using control and KO cells grown under hypoxic conditions (Fig-

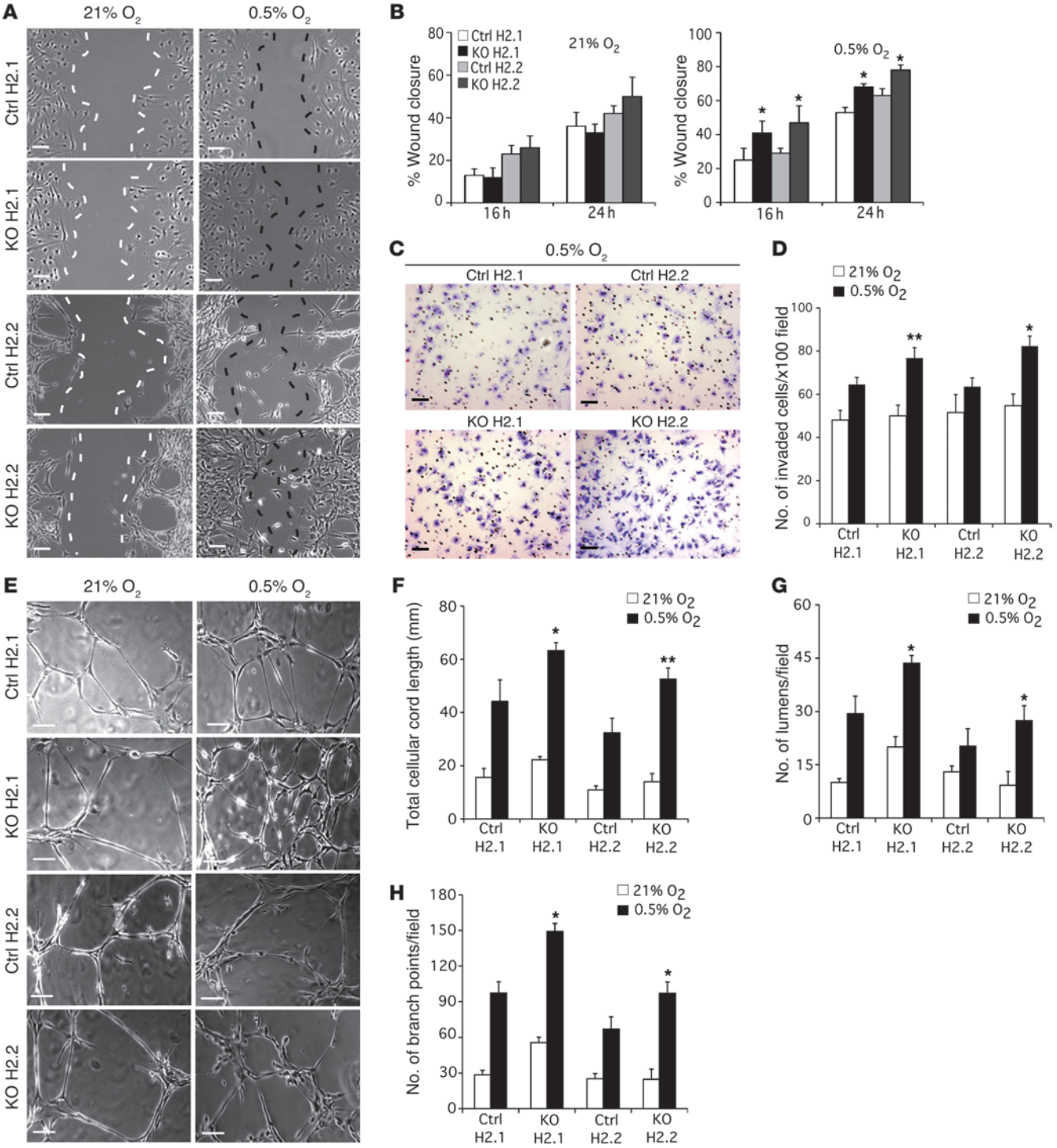

Figure 4

HIF-2α deletion affects EC migration and network formation. (**A**) Migration of control and KO lung ECs was assessed under normoxic (21% O_2) or hypoxic (0.5% O_2) conditions at several time points using a scratch wound assay. Representative images were taken 24 hours after scratch. Ctrl H2.1 and KO H2.1, control and HIF-2α KO ECs. Ctrl H2.2 and KO H2.2, control and KO ECs with an acute deletion of HIF-2α (Tamoxifen induced). (**B**) Percent wound closure, determined at consistent locations, was significantly increased for KO ECs 16 and 24 hours after scratch and under hypoxic conditions. (**C**) EC invasion was further assessed using a Boyden chamber assay. Images represent control and KO EC invasion after 8 hours under hypoxic conditions. (**D**) Number of invaded cells was quantified after 8 hours under normoxic or hypoxic conditions. Increased invasion was observed for KO ECs compared with control under hypoxic conditions. (**E**) EC network/capillary formation was assessed using a Matrigel assay. Images represent control and KO EC capillary formation after 8 hours under normoxic or hypoxic conditions. (**F**–**H**) Quantifications of EC network formation revealed significant increase in total cellular cord length (**F**), number of lumens (**G**), and branch points (**H**) for KO versus control ECs under hypoxic conditions. Original magnification, ×100. Scale bars: 30 μm. Experiments were performed in triplicate. *$P < 0.05$; **$P < 0.01$.

ure 6). Interestingly, control ECs treated with DAPT exhibited increased cell network/capillary formation (Figure 6, A–D) as well as increased migratory and invasive phenotypes (Figure 6, E–G), achieving levels similar to those observed for untreated KO ECs. Consistent with these results, DAPT treatment reduced the adhesion of control HIF-2α–replete ECs to Matrigel or fibronectin-coated plates to levels indistinguishable from those of untreated KO ECs (Supplemental Figure 8, D and E).

In a complementary gain-of-function experiment, control and KO ECs were plated on tissue culture dishes coated with Fc-Dll4 fusion protein (Figure 7). In contrast to soluble Fc-Dll4 protein, which acts as a Notch inhibitor, immobilized Fc-Dll4 protein has been shown to activate Notch signaling (33, 34). The elevated migratory behavior of hypoxic KO ECs was diminished by exposure to Fc-Dll4 ligands (Figure 7, A and B). Control ECs exposed to Fc-Dll4 similarly displayed a slight decrease in migration, also to levels comparable to KO ECs (Figure 7B). Western blot and qRT-PCR analysis confirmed that the Fc-Dll4 ligand activated Notch signaling, as levels of NICD protein and *Hes1* and *Hey2* mRNA were strongly induced in hypoxic control and KO ECs (Figure 7, C and D). These results implicate the Dll4/Notch pathway as a principal downstream target of HIF-2α function in ECs in pathophysiological angiogenesis and arteriogenesis.

Exogenously supplied Dll4 and Ang2 rescue angiogenic phenotypes of HIF-2α–deficient ECs in vivo. To confirm Dll4/Notch signaling as a physiologically relevant downstream effector of HIF-2α function in ECs, we repeated the FAL procedure, but injected surgically exposed KO adductor muscle with adenovirus-associated virus (AAV) engineered to express Dll4 protein. Experiments using control AAV vector encoding GFP revealed extensive expression in muscle fibers and ECs (Supplemental Figure 9A). Whereas injection of control AAV vector had no effect on recovery of limb perfusion in control or KO mice, injection of virus expressing Dll4 protein (Supplemental Figure 9B) largely restored blood flow in ischemic KO muscle to control levels by 7–14 days postsurgery (Figure 8 and Supplemental Figure 10, A and B). Additional postoperative intravenous injection of soluble recombinant Ang2 protein augmented the effects of Dll4 expression, fully restoring blood flow in ischemic KO limbs to control levels (Figure 8B). Concomitant changes in collateral artery diameter (Figure 8, C and D), relative tissue injury (Figure 8, E and F), capillary density and vascular area (Figure 8, G–I), and foot movement and necrosis (Supplemental Figure 10, C and D) were also observed in KO mice treated with Dll4 and Ang2. These data strongly suggest that Dll4 and Ang2 are critical HIF-2α effectors required to regulate effective compensatory angiogenesis in ischemic tissue.

Discussion

Angiogenesis and vascular remodeling are highly complex, dynamic processes strongly influenced by hypoxia and other microenvironmental stimuli (1). Multiple studies have revealed that the oxygen-responsive HIF transcriptional factors HIF-1α and HIF-2α are important regulators of pathological angiogenesis (10), although the precise mechanisms by which they coordinate vessel sprouting and remodeling remain unclear. In the current work, we identified unique cell-autonomous functions for HIF-2α in regulating EC behavior and demonstrated that EC-specific HIF-2α deletion in mice impaired angiogenesis in hindlimb ischemia and autochthonous solid tumor models. It is interesting to note that, although reduced HIF-1α expression also disrupted angiogenesis in these disease models, there were striking phenotypic differences between HIF-1α– and HIF-2α–deficient mice.

HIF-1α and HIF-2α share many target genes, but mounting evidence indicates that each protein fulfills distinct, and sometimes opposing, physiological functions in specific cell types, including ECs (35). For example, hypoxic VEGF expression is driven primarily by HIF-1α in ECs, whereas hypoxic Dll4 and Ang2 expression is regulated primarily by HIF-2α, suggesting an important division of transcriptional labor that underlies complementary effects on EC behavior. HIF-1α–null ECs cultured under hypoxic conditions exhibit reduced proliferation, VEGF expression, migration, and cytoplasmic cord formation (16). In contrast, the HIF-2α–deficient ECs of our KO mice displayed no significant differences in proliferation rates or VEGF expression, but instead exhibited significantly enhanced branching, migration, and invasion. Moreover, pathophysiological angiogenesis in KO mice was characterized by increased vessel density, but poor arteriogenesis and reduced perfusion, resulting in increased ischemic damage or reduced autochthonous tumor growth. Using both in vitro and in vivo techniques, we identified Dll4 and Ang2 as critical downstream effectors of HIF-2α function in ECs and further demonstrated that exogenous Dll4 and Ang2 expression was sufficient to fully restore perfusion in ischemic muscle with HIF-2α–deficient ECs.

Taken as a whole, the available data are consistent with a model in which HIF-1α promotes EC growth, proliferation, and morphogenesis in response to local hypoxic stress; however, these activities are restrained and fine-tuned by HIF-2α to promote vessel remodeling and produce a mature, functional vascular network (Figure 9). In previous reports, the effects of HIF-1α on angiogenesis in the FAL model were attributed primarily to the mobilization of circulating angiogenic cells (14, 36), and Takeda et al. demonstrated that *Phd2*$^{+/-}$ mice were protected against hindlimb ischemia through modulation of macrophage populations, which regulate arteriogenesis (37). We are currently investigating whether HIF-2α regulates the recruitment of these cells to sites of pathological angiogenesis in our models; however, the EC-intrinsic effects on Dll4 and Ang2 appear to account for the majority of the phenotypes observed. Nevertheless, additional HIF-2α target genes almost certainly play important roles in pathophysiological angiogenesis. It would be of considerable interest to subject mice with EC-specific loss of both HIF-1α and HIF-2α to similar ischemia and tumor growth experiments, although an inducible deletion strategy would likely be required, as EC-specific deletion of the murine gene encoding HIF-1β produces embryonic and perinatal lethality associated with altered liver function (38).

Our data are consistent with other reports demonstrating that HIF-1α and HIF-2α can promote opposing cellular responses in specific settings. Examples include inhibition or augmentation of c-Myc transcriptional activity in renal cell carcinomas (by HIF-1α or HIF-2α, respectively; ref. 11) and elevated or diminished nitric oxide production in macrophages (by HIF-1α or HIF-2α, respectively; refs. 13, 39, 40). These and other data (41) make it increasingly clear that HIF-1α and HIF-2α mediate hypoxic responses by acting either in concert or in opposition, depending on the precise physiological setting. This model also suggests that therapeutic targeting of the HIF pathway may require independent regulation of each isoform, depending on the specific pathological context (42).

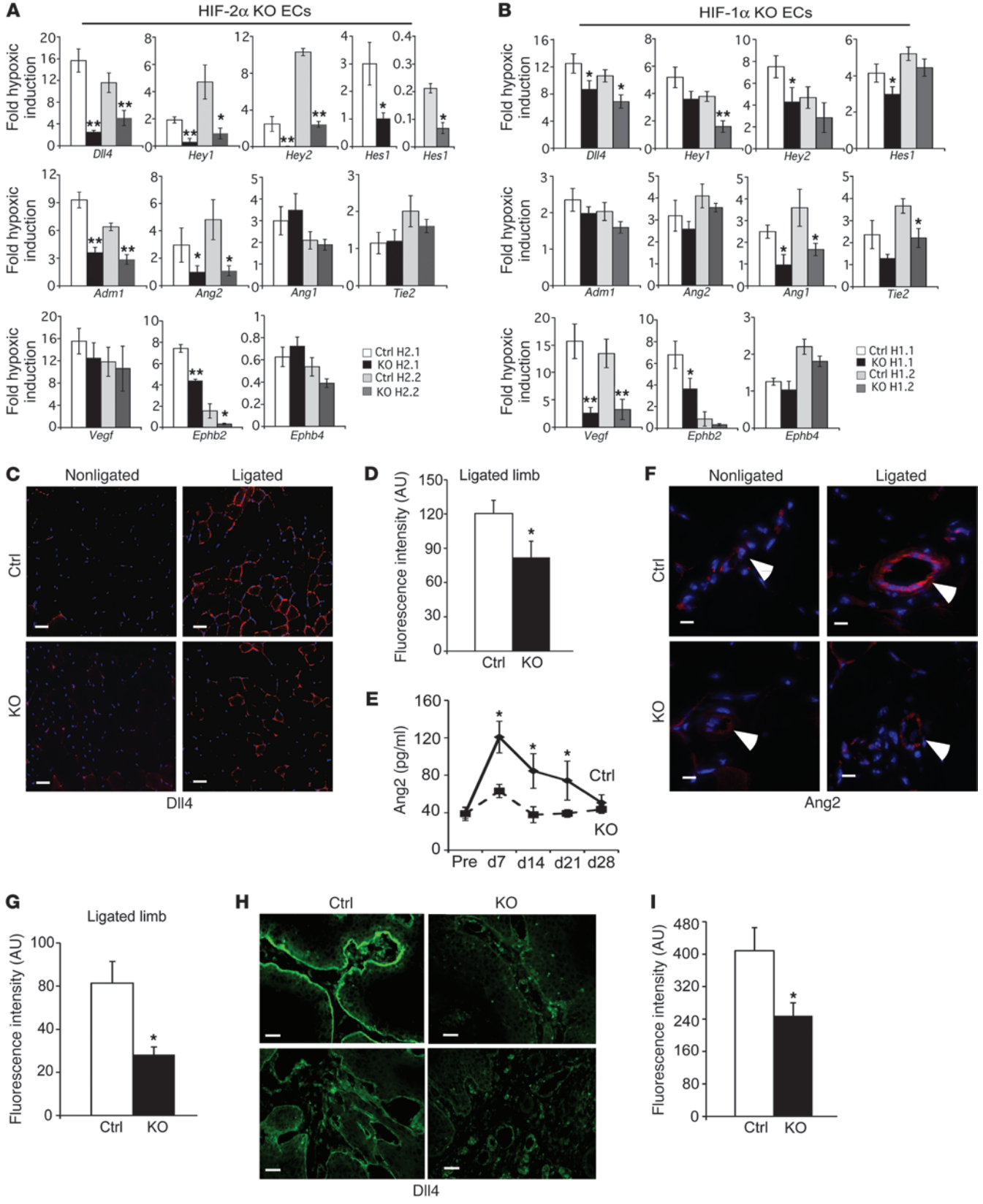
A
HIF-2α KO ECs
Fold hypoxic induction
Dll4
Hey1
Hey2
Hes1
Hes1
Adm1
Ang2
Ang1
Tie2
Vegf
Ephb2
Ephb4
Ctrl H2.1
KO H2.1
Ctrl H2.2
KO H2.2
B
HIF-1α KO ECs
Fold hypoxic induction
Dll4
Hey1
Hey2
Hes1
Adm1
Ang2
Ang1
Tie2
Vegf
Ephb2
Ephb4
Ctrl H1.1
KO H1.1
Ctrl H1.2
KO H1.2
C
Nonligated
Ligated
Ctrl
KO
Dll4
D
Ligated limb
Fluorescence intensity (AU)
Ctrl
KO
E
Ang2 (pg/ml)
Ctrl
KO
Pre
d7
d14
d21
d28
F
Nonligated
Ligated
Ctrl
KO
Ang2
G
Ligated limb
Fluorescence intensity (AU)
Ctrl
KO
H
Ctrl
KO
Dll4
I
Fluorescence intensity (AU)
Ctrl
KO

Figure 5
Endothelial HIF-2α deficiency impairs hypoxic induction of angiogenic genes. (**A** and **B**) Hypoxic induction of HIF and Dll4/Notch pathway target gene expression was assessed by qRT-PCR in control, HIF-2α (**A**), and HIF-1α (**B**) KO lung ECs. The relative ratio of hypoxic to normoxic gene expression (fold hypoxic induction) is shown for control and KO ECs (n = 6). Note that Hes1 charts for HIF-2α KO ECs were separated for the 2 replicates. (**C**) Dll4 staining in adductor muscle for ligated and nonligated limb in control and KO mice at day 7 after surgery. (**D**) Quantification of fluorescence intensity revealed decreased Dll4 expression in the ligated limb of KO mice after ligation. (**E**) Levels of Ang2 were assessed in control (n = 8) and KO (n = 9) serum after ligation. (**F**) Ang2 staining in adductor muscle for ligated and nonligated limb in control and KO mice at day 7 after surgery. Arrowheads denote collaterals. (**G**) Quantification of fluorescence intensity revealed decreased Ang2 expression in the ligated limb of KO mice. (**H**) Dll4-immunofluorostained sections of skin tumors from control and KO mice after 25 weeks of DMBA/TPA treatment. (**I**) Quantification of fluorescence intensity revealed decreased Dll4 expression in skin tumors of KO mice (n = 10 [control]; 11 [KO]). Scale bars: 40 μm (**C** and **H**); 20 μm (**F**). Original magnification, ×200. $^*P < 0.05$; $^{**}P < 0.01$.

Our data also revealed HIF-2α as the primary activator of hypoxic Dll4/Notch signaling in ECs, adding an interesting facet to the complex relationship between these important regulatory pathways. The Dll4/Notch pathway is required for angiogenesis in peripheral ischemia models; for example, blood flow recovery and postnatal neovascularization in response to hindlimb ischemia are impaired in *Notch1*$^{+/-}$ or *Dll1*$^{+/-}$ mice (43). Additionally, Dll4 inhibition impairs reparative angiogenesis after ischemia by the formation of a disorganized, low-perfused capillary network in ischemic muscles (31) and causes proliferation of nonfunctional vessels in xenograft tumors, resulting in poor perfusion and reduced tumor growth (21). These phenotypes are remarkably similar to those observed in our FAL and papilloma experiments, and we further demonstrated that enforced Dll4/Notch signaling largely reversed the impaired recovery from FAL in our KO mice.

Previous analysis demonstrated that Dll4 inhibition promoted the formation of vascular tip cells at the expense of proliferative stalk cells, resulting in vascular discontinuity and leakage (44, 45). Initial attempts to investigate the relative presence of tip and stalk ECs in ischemic muscles and papillomas of our control and KO animals were inconclusive, as were attempts to quantify these cells using a more tractable oxygen-induced retinopathy (OIR) model (ref. 46 and data not shown). The equivocal OIR results may reflect the mixed genetic background of the mice (47); consequently, we intend to repeat these experiments using mice that have been repeatedly backcrossed onto the C57BL/6 genetic background. It is also interesting to note that HIF-2α–deficient ECs have reduced expression of VEGFR2 (18), which collaborates with Dll4/Notch signaling to regulate tip and stalk cell fate (48). Whether HIF-2α, Dll4/Notch signaling, or both regulate VEGFR2 expression in tip and stalk cells is in interesting question for future study.

Hypoxia has previously been reported to regulate Notch pathway activity through direct and indirect mechanisms in other settings. For example, HIF-1α binds NICD directly in stem and progenitor cells, promoting NICD stabilization and increased target gene expression (49). Reduced HIF-1α expression has been shown to correlate with decreased NICD levels and activity in thymic lymphomas from *Hif1a*$^{+/-}$*p53*$^{R270/R270}$ mutant mice (50), and mRNA and protein levels of Notch1 are induced by hypoxia in a HIF-1α–dependent manner in melanoma cells (51). Moreover, ectopically expressed HIF-1α and HIF-2α activate the expression of genes encoding Dll4, Hey1, and Hey2 in endothelioma and endothelial precursor cells, although this regulation may be independent of direct HIF DNA binding activity (26). Interestingly, ADM1 is an established HIF-2α target and has also been shown to activate the Notch pathway, providing another potential link between hypoxia and Notch signaling in ECs (28). It is also possible that HIF and Notch pathways collaborate in stromal cells, such as pericytes and smooth muscle cells, to regulate angiogenesis and vascular function.

Determining the complex effects of local hypoxia on pathological angiogenesis is likely to have important therapeutic consequences (52). The ability to induce and regulate angiogenesis and vascular remodeling in a directed manner would represent a major advance in the treatment of ischemic vascular diseases, including myocardial infarction, atherosclerosis, and PAD, which constitute a major cause of death and morbidity in industrialized societies (53). Although angioplasty, bypass grafting, and other therapies are partly successful in restoring blood flow to affected tissues, there are currently no effective strategies to selectively generate new functional vessels to relieve ischemic stress, which can otherwise produce severe tissue necrosis and gangrene and necessitate amputation. In contrast, inhibiting angiogenesis with targeted therapies has shown some efficacy in treating solid tumors and macular degeneration, maladies typically associated with unregulated or excessive angiogenic activity (2). For example, the humanized VEGF antibody bevacizumab is an FDA-approved treatment for macular degeneration, in addition to being a first-line therapy for colon and non–small cell lung cancer (54). Similarly, the small-molecule VEGFR inhibitors sunitinib and sorafenib are approved for the treatment of renal carcinomas, as well as gastrointestinal stromal tumors and hepatocellular carcinomas, respectively (55). By elucidating the molecular mechanisms controlling endogenous responses to the hypoxic stress associated with ischemic attack and tumor growth, we hope to reveal novel targets with which to regulate angiogenesis therapeutically.

Methods

Generation of conditional HIF-2α VE-cadherin–Cre mice. To delete HIF-2α function in ECs, mice carrying the conditional *Hif2a*^{fl} allele (18, 23) were bred to transgenic mice expressing Cre recombinase under the control of the VE-cadherin promoter (56) to obtain experimental KO mice (*Hif2a*$^{fl/\Delta}$*Cre*) and controls (*Hif2a*$^{fl/+}$*Cre*). All mice were maintained in a mixed Sv129/C57BL6 genetic background. *Hif2a* wild-type (+), conditional floxed (fl), and deleted (Δ) genomic alleles were distinguished using a multiplex PCR as described previously (18).

Hindlimb ischemia model. We assessed blood flow and oxygenation values before and after FAL in 42 mice (22 KO; 20 control) about 9 months of age weighing 25–30 g. Mice were anesthetized using intraperitoneal injection of avertin (2, 2, 2-tribromoethanol; Sigma-Aldrich) prepared as a 1.2% solution at a dosage of 0.2 ml/10 g body weight, which approximates 240 mg/kg. Unilateral FAL was performed as described previously (57, 58). Briefly, the left femoral artery was exposed, isolated from the femoral nerve and vein, and ligated distally to the origin of the arteria profunda femoris. The skin was finally closed by interrupted 4-0 sutures (Syneture). Follow-up hemodynamic measurements were carried out postoperatively once a week over 4 weeks.

Speckle imaging, blood flow, and oxygenation assessment. Efficiency of FAL was determined in adductor muscles and feet using Speckle imaging techniques right after surgery. Relative blood flow was also measured by LD and DCS as described previously (22). Measurements were performed

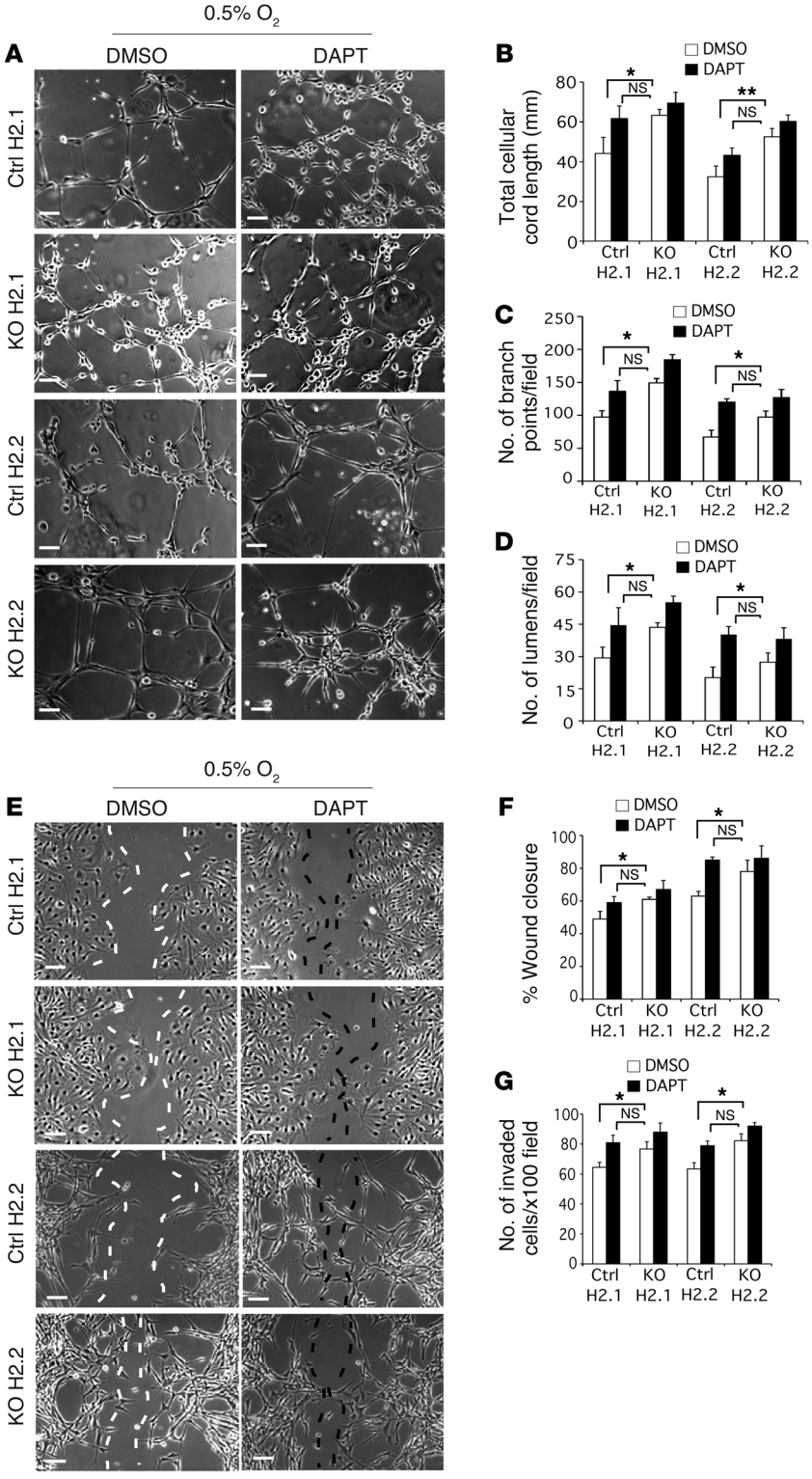

Figure 6

Notch pathway inhibition phenocopies HIF-2α deficiency in EC network formation and migration. (**A**) EC network/capillary formation was assessed using a Matrigel assay. Images show control and KO ECs after 8 hours under hypoxic conditions and treated with DAPT. (**B**–**D**) Quantification of EC network formation revealed no significant difference in total cellular cord length (**B**) and number of branch points (**C**) and lumens (**D**) between untreated KO ECs and DAPT-treated control cells under hypoxic conditions. (**E**) Migration of control and KO lung ECs treated with DAPT was assessed under hypoxic conditions at several time points using a scratch wound assay. Representative images were taken 16 hours after scratch. (**F**) Percent wound closure showed no significant difference between untreated KO ECs and DAPT-treated control cells at 16 hours after scratch and under hypoxic conditions. (**G**) EC invasion was further assessed using a Boyden chamber assay after 8 hours under hypoxic conditions and treatment or not with DAPT. The number of invaded cells showed no significant invasion difference between untreated KO ECs and DAPT-treated control cells under hypoxic conditions. Original magnification, ×100. Scale bars: 30 μm. Experiments were performed in triplicate. $^{*}P < 0.05$; $^{**}P < 0.01$.

pre– and post–artery ligation, and additionally on postoperative days 7, 14, 21, and 28. The left limb/right limb ratio (ligated/nonligated leg) was calculated for each animal. Oxygen saturation was determined by diffuse reflectance spectroscopy/white-light spectroscopy, which provides the absolute concentrations of oxy- and deoxyhemoglobin through the Beer-Lambert law as described previously (22).

Foot movement score and necrosis assessment. To assess functional limb recovery, we used the following scoring system based on active foot movement of individual mice: 4, unrestricted movement; 3, use of complete foot or spreading of toes; 2, active foot use; 1, use of the leg; 0, dragging of foot. We also scored the severity of necroses in control and KO animals to assess mice that had to be euthanized during the course of the experiment.

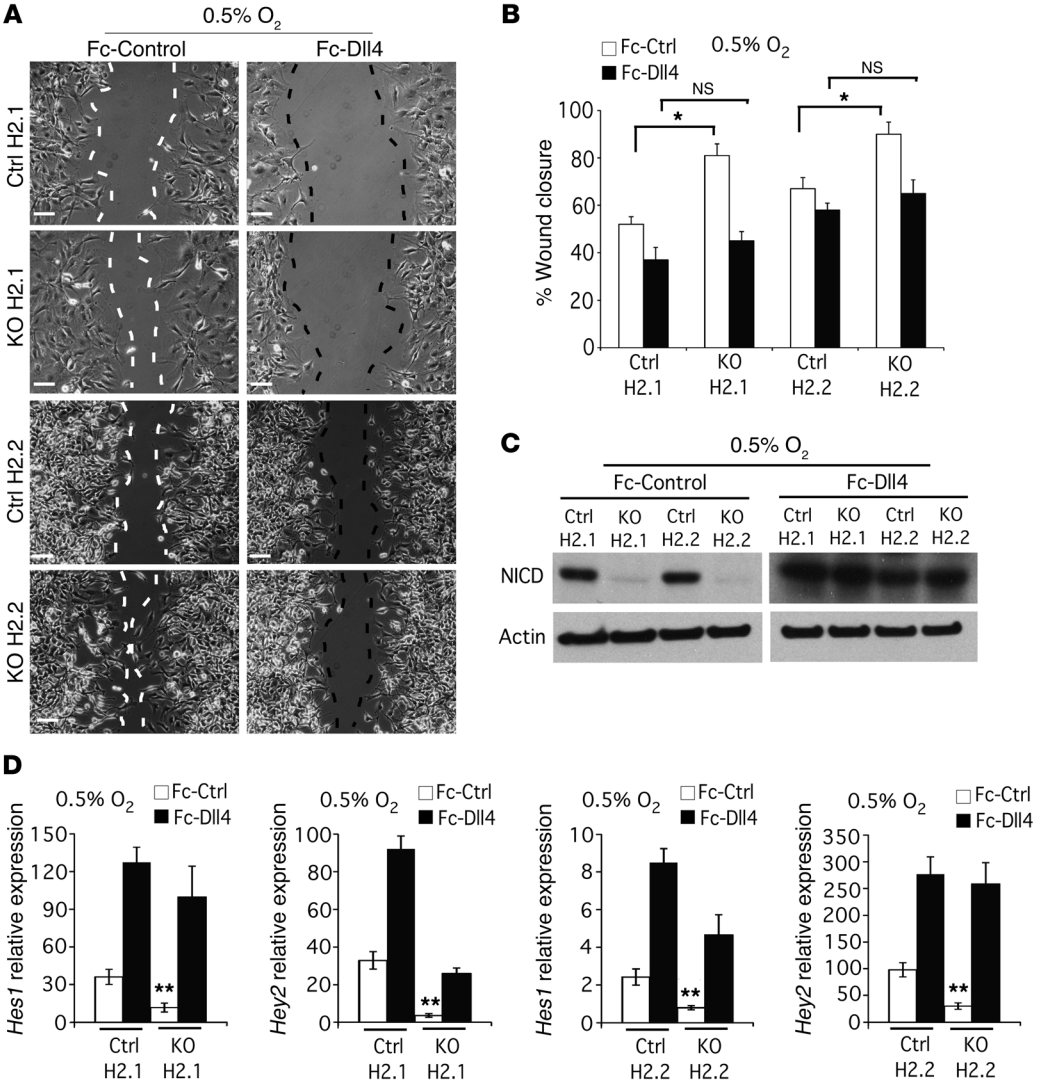

Figure 7

HIF-2α deletion affects EC migration through the Dll4/Notch pathway. (**A**) Migration of control and KO lung ECs was assessed on control- or Dll4-coated plates under hypoxic conditions at several time points using a scratch wound assay. Representative images were taken 24 hours after scratch. Original magnification, ×100. Scale bars: 100 μm. (**B**) Percent wound closure showed no significant difference between KO and control ECs on Dll4-coated plates at 24 hours after scratch and under hypoxic conditions. (**C**) Western blot analysis of NICD protein expression in control and KO ECs seeded on control- or Dll4-coated plates under hypoxic conditions. (**D**) Induction of Dll4/Notch pathway target genes expression *Hes1* and *Hey2* was assessed by qRT-PCR in control and KO lung ECs seeded on control- or Dll4-coated plates under hypoxic conditions. Experiments were performed in triplicate. $^{*}P < 0.05$; $^{**}P < 0.01$.

ELISA and creatine kinase assay. Human Ang2 ELISA (R&D Systems) and creatine kinase assay (Bioassay Systems) were performed according to the instructions of the manufacturer. Blood was obtained by retro-orbital puncture at different time points.

qRT-PCR analysis. Total RNA was isolated from purified ECs grown under normoxic (21% O_2) conditions, or exposed to 16 hours of hypoxic (0.5% O_2) conditions, using TRIzol reagent (Invitrogen). Primers for specific transcripts were purchased from Applied Biosystems (see Supplemental Methods). qRT-PCR was performed on EC RNAs using Syber Green PCR Master Mix (Invitrogen) and the Applied Biosystems 7900HT Sequence Detection System (TaqMan). β-actin or 18S rRNA was used as endogenous control in the ΔδCt analysis.

Immunohistochemistry and immunofluorescence. Tissue sampling and morphometric analysis of collateral artery growth and capillary formation were performed as described previously (59, 60). Briefly, on day 7, 14, 21, or 28 after FAL surgery, the remaining animals were sacrificed by CO_2 inhalation and perfused with PBS (Lonza) followed by 3.7% paraformaldehyde intracardially. For vascular studies, mice were anesthetized with avertin and injected with 100 μl of 1 mg/ml rhodamine (Griffonia Simplicifolia) and lectin (Vector Laboratories) in PBS intravenously via the tail vein, after which mice were perfused with PBS intracardially. The adductor muscles were dissected, sucrose immersed, embedded in OCT compound (Sakura Finetek), frozen using a liquid nitrogen and isopentane bath, and sectioned using a cryostat (sections of 10–15 μm). Some adductor muscles were also

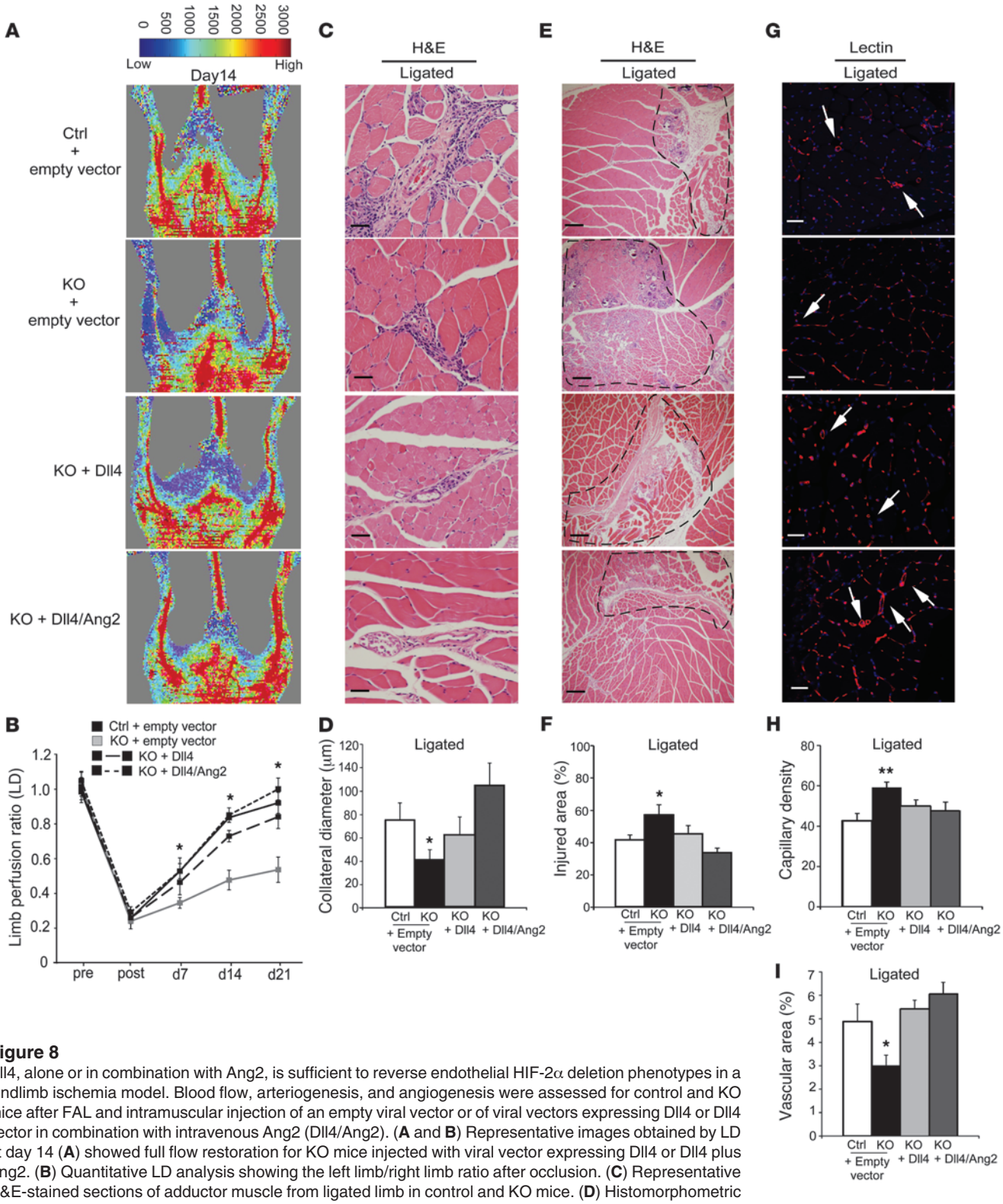

Figure 8

Dll4, alone or in combination with Ang2, is sufficient to reverse endothelial HIF-2α deletion phenotypes in a hindlimb ischemia model. Blood flow, arteriogenesis, and angiogenesis were assessed for control and KO mice after FAL and intramuscular injection of an empty viral vector or of viral vectors expressing Dll4 or Dll4 vector in combination with intravenous Ang2 (Dll4/Ang2). (**A** and **B**) Representative images obtained by LD at day 14 (**A**) showed full flow restoration for KO mice injected with viral vector expressing Dll4 or Dll4 plus Ang2. (**B**) Quantitative LD analysis showing the left limb/right limb ratio after occlusion. (**C**) Representative H&E-stained sections of adductor muscle from ligated limb in control and KO mice. (**D**) Histomorphometric analysis of collateral lumen showing rescue in collateral diameter by Dll4 expression and the combination of Dll4 and Ang2. (**E**) H&E-stained sections of adductor muscle for ligated limb in control and KO mice injected as indicated. Dashed outlines denote damaged or injured areas within muscle. (**F**) Percent injured area per section for ligated limb in control and KO mice. (**G**–**I**) Rhodamine-lectin staining (**G**) showed decreased vessel density (**H**) and increased vascular area (**I**) in adductor muscle of KO mice injected with Dll4 alone or in combination with Ang2. Arrows indicate capillaries. Scale bars: 20 μm (**C** and **G**); 80 μm (**E**). Original magnification, x200 (**C**); x100 (**E**); ×400 (**G**). $n = 20$ per group. $^{*}P < 0.05$; $^{**}P < 0.01$.

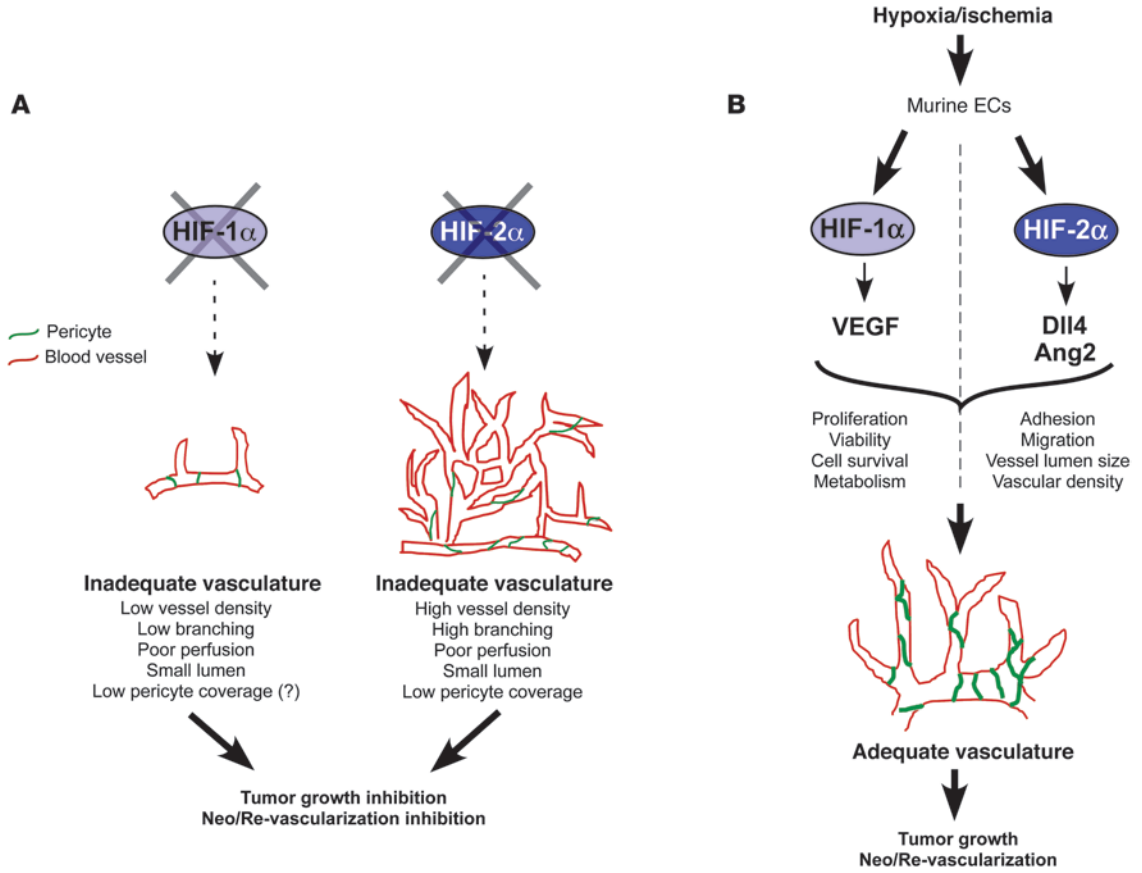

Figure 9
Unique cell-autonomous functions for HIF-2α in physiological and pathophysiological angiogenic processes. (**A**) Inhibiting either HIF-1α or HIF-2α in ECs leads to an inadequate vasculature by different mechanisms, but results in the same consequences on tumor growth and vascularization processes. (**B**) Model of HIF-1α and HIF-2α functions in murine ECs in response to hypoxia/ischemia, reflecting unique transcriptional targets of HIF-1α and HIF-2α. HIF-1α and HIF-2α fulfill complementary, and largely nonoverlapping, essential functions in physiological and pathophysiological angiogenesis.

dissected, fixed in 3.7% paraformaldehyde for 48 hours, and embedded in paraffin before sectioning. Sections were stained with H&E and mounted in Fluoromount-G media (Southern Biotech) for morphometric analyses. Immunofluorescent staining was performed using a standard immunofluorescent protocol as described previously (43). Sections were counterstained using DAPI (Vector), and vasculature in tissue sections from control and KO mice was visualized using rhodamine-lectin staining. The number of vessels and the vascular area were measured as described previously (59). Vascular area was determined as the combined area of rhodamine-labeled vessels plus lumens in 5 independent fields and expressed as a percentage of the total image area. The degree of mural cell coverage was visualized by FITC-conjugated smooth muscle actin antibody. Fluorescence was also quantified using color thresholding techniques in Metamorph software (Molecular Devices), and values were expressed as a percentage of the entire image area. Images were acquired under the same conditions for each experiment, and no digital manipulation of images was performed other than cropping and merging. Image analyses and quantifications were performed using a Leica 500 microscope (Leica) as well as ImageJ and Metamorph software (Molecular Devices), as described previously (60).

Skin tumor induction protocol. For tumor induction, mice were initiated with a dose of 25 μg of 7,12-dimethylbenz(a)anthracene (DMBA; Sigma-Aldrich) in 200 μl of acetone applied to the dorsal surface 2 days after shaving. 12.5 μg of 12-O-tetradecanoylphorbol-13-acetate (TPA; Sigma-Aldrich) in 200 μl of acetone, was applied every week for 25 weeks beginning 1 week after initiation. The appearance of lesions, incidence, size and multiplicity in each mouse was monitored every week. Tumor multiplicity was calculated as the average number of skin tumors per mouse. Tumor incidence was calculated as the percentage of mice with skin tumors. Dorsal skin and/or tumors were dissected from euthanized mice and embedded in OCT compound (Sakura Finetek), frozen using a liquid nitrogen and isopentane bath, and sectioned using a cryostat (sections of 5–10 μm). For vasculature study, tumor-bearing mice were anesthetized with avertin and injected with 100 μl of 1 mg/ml rhodamine-lectin in PBS intravenously into the tail vein, after which mice were perfused with PBS intracardially before dissection. Sections were stained with H&E for histopathological analyses or processed using a standard immunofluorescent protocol as described previously (43). Briefly, sections were washed in PBS. Antigen unmasking was performed in a pressure cooker in citrate buffer (Vector Laboratories). Sections were blocked with a blocking solution consisting of 4% BSA and 2% normal goat serum in TT buffer (30 mM Tris, pH 7.2; 140 mM sodium cacodylate) and immunostained using the appropriate antibody in the blocking solution overnight at 4°C. Secondary antibodies labeled with Alexa Fluor 488 or Alexa Fluor 546 (Invitrogen) were placed on tissue sections for 1 hour at room temperature. Sections were counterstained using DAPI (Vector) and mounted in Fluoromount-G media (Southern Biotech).

EC isolation, characterization, and culture. Murine endothelial MS1 cells were obtained from ATCC. For the functional assays, cells were treated with DMSO (Sigma-Aldrich) or DAPT (10 μM; Sigma-Aldrich). Immortalized EC populations were generated from lung, skin, and adductor tissues of HIF-1α/HIF-2α KO and control mice as described previously (25, 61), with minor modifications. ECs used for the acute deletion experiments were generated from lung tissues of *Hif2a*$^{fl/\Delta}$*Ubc-CreER* (23) and *Hif1a*$^{fl/fl}$*Ubc-CreER*, animals. Briefly, lungs from control or KO mice were macerated in sterile PBS, filtered through a 75-μM mesh and digested with collagenase (Stem Cell Technologies Inc.) at 37°C for 1 hour as described previously (61). Following hemolysis with ACK buffer (150 mM NH_4Cl; 10 mM $KHCO_3$; 0.1 mM Na_2EDTA, pH 7.4) for 5 minutes at room temperature, cells were pelleted, resuspended in EGM media (Lonza), and plated on fibronectin-coated 35-mm^2 plates (R&D Systems). Confluent cultures were trypsinized and incubated with CD31 antibody–conjugated Dynal beads (Invitrogen). Selected cells were replated, then immortalized by infection with the pMigR1 vector encoding GFP-conjugated polyomavirus middle T antigen. Immortalized cells were subjected to 2 additional rounds of CD31 and 1 of ICAM-2 selection. Purity of the ECs was determined by their ability to take up Dil-Ac-LDL (10 μg/ml; Biomedial Technology Inc.) or by flow cytometry (FACS Scan; BD) after phycoerythrin-CD31 staining (BD Biosciences — Pharmingen).

Migration/in vitro wound closure assay. For the wound closure assay, cells were seeded in 6-well plates and incubated overnight to generate confluent cultures. Cell layers were scraped with a plastic pipette tip and washed 3 times with serum-free medium. The remaining cell culture was incubated for 48 hours to allow cells to migrate into the cleared space. To quantify cell migration, phase-contrast images of identical locations in each wound were taken at 0, 8, 16, 24, and 48 hours after wounding. The rate of cell migration was then calculated as the average percent wound closure from at least 3 independent experiments using an Olympus IX81 microscope (Olympus) and ImageJ software.

Dll4/Notch pathway induction. In vitro, the Dll4/Notch pathway was activated by exposing cells to immobilized ligand. First, 293T cells were transfected with plasmids encoding fusion proteins between Fcγ of control IgG (Fc-Control) and the extracellular domain of Dll4 (Fc-Dll4; provided by T. Kadesch, Perelman School of Medicine at the University of Pennsylvania, Philadelphia, Pennsylvania, USA). Conditioned medium was collected. Culture plates were initially coated for 1 hour at room temperature with 10 mg/ml anti-Fc antibody (Jackson Immunoresearch). The anti-Fc/PBS solution was then aspirated and replaced by filtered conditioned medium described above. After 1 hour of incubation, supernatant was aspirated, and cells were plated for the migration/in vitro wound closure assay.

To express recombinant Dll4 in skeletal muscle tissue, a full-length Mammalian Gene Collection (MGC) verified Dll4 cDNA was obtained from Open Biosystems (MMM1013-9498507; clone 6825525) in a pYX-Asc plasmid. This plasmid was cloned into an AAV *cis* plasmid by the Penn Vector Core (www.med.upenn.edu/gtp/vectorcore) and used to generate AAV2/9 viral particles containing *Dll4* under the expression of the CMV promoter. High-titer experimental AAV2/9.CMV.PI.mDLL4.RBG virus (8.84×10^{12} genomic copies/ml) and control AAV2/9.CMV.EGF.bGH virus (1.95×10^{13} genomic copies/ml) was used in subsequent FAL experiments. Control and KO mice were randomly assigned to receive either EGF (control) virus or DLL4-expressing virus, which was injected at 4 sites in the ligated limb (specifically, the anterior and posterior thigh muscles at superior and inferior positions) immediately following surgical occlusion. Each mouse received 1 set of injections, each of which delivered 10^{11} genomic copies of virus diluted in PBS to 25 μl. Viral transgene expression was verified in tissues by immunofluorescence. Additionally, recombinant Ang2 (50 μg; R&D Systems) or PBS was provided to appropriate treatment groups by tail vein injection at 3 time points: immediately after ligation, 1 day after ligation, and 2 days after ligation.

Cord formation assay. Growth factor–reduced Matrigel (300 μl; BD) was added to each well of a 24-well plate and allowed to polymerize for 1 hour at 37°C. A total of 1×10^5 cells, preincubated with serum-free EGM media for 1 hour, was seeded. Cells were incubated for 8 hours at 21% or 0.5% O_2, viewed, photographed, and quantified using a Leica 500 microscope (Leica) as well as ImageJ and Metamorph software (Molecular Devices). The number of cords was measured by counting the number of cytoplasmic extensions, and the number of branch points, visible lumens, and total cord length were also determined. At least 3 fields per well were examined, and each experimental condition was tested in triplicate.

Statistics. Comparison of multiple groups was performed by ANOVA. 2-group analysis was performed by 1-tailed Student's *t* test. Results shown represent average ± SEM of 6–9 samples from 2–3 independent studies. Error bars represent SEM for all figures. A *P* value less than 0.05 was considered significant.

Study approval. Experiments were conducted in accordance with NIH guidelines for the use and care of live animals and were approved by the University of Pennsylvania IACUC.

Acknowledgments

We thank Hongwei Yu for histological preparations; the M.C. Simon laboratory for helpful discussions and comments; Tom Kadesch for providing the Fc-Dll4 plasmid; and Regina Choe and the Joel Greenberg laboratory for their collaboration, particularly Wes Baker for his technical assistance. This work was funded by the Howard Hughes Medical Institute and the NIH (grants R01-NS060653, HL66130, and RR02305). M.C. Simon is an investigator of the Howard Hughes Medical Institute.

Received for publication December 23, 2011, and accepted February 3, 2012.

Address correspondence to: M. Celeste Simon, Howard Hughes Medical Institute, Abramson Family Cancer Research Institute, Department of Cell and Developmental Biology, Perelman School of Medicine at the University of Pennsylvania, 456 BRB II/III, 421 Curie Boulevard, Philadelphia, Pennsylvania 19104-6160, USA. Phone: 215.746.5532; Fax: 215.746.5511; E-mail: celeste2@mail.med.upenn.edu.

Anja Runge's present address is: Division of Vascular Oncology and Metastasis, German Cancer Research Center, Heidelberg, Germany.

Liping Liu's present address is: Merck Research Laboratories, West Point, Pennsylvania, USA.

1. Carmeliet P. Angiogenesis in life, disease and medicine. *Nature*. 2005;438(7070):932–936.
2. Zhou B, Poon MC, Pu WT, Han ZC. Therapeutic neovascularization for peripheral arterial diseases: advances and perspectives. *Histol Histopathol*. 2007;22(6):677–686.
3. Roodink I, Leenders WP. Targeted therapies of cancer: angiogenesis inhibition seems not enough. *Cancer Lett*. 2010;299(1):1–10.
4. Zachary I, Morgan RD. Therapeutic angiogenesis for cardiovascular disease: biological context, challenges, prospects. *Heart*. 2011;97(3):181–189.
5. Bertout JA, Patel SA, Simon MC. The impact of O2 availability on human cancer. *Nat Rev Cancer*. 2008;8(12):967–975.
6. Majmundar AJ, Wong WJ, Simon MC. Hypoxia-inducible factors and the response to hypoxic stress. *Mol Cell*. 2010;40(2):294–309.
7. Wang GL, Semenza GL. Purification and characterization of hypoxia-inducible factor 1. *J Biol Chem*. 1995;270(3):1230–1237.

8. Tian H, McKnight SL, Russell DW. Endothelial PAS domain protein 1 (EPAS1), a transcription factor selectively expressed in endothelial cells. *Genes Dev*. 1997;11(1):72–82.
9. Maynard MA, et al. Multiple splice variants of the human HIF-3 alpha locus are targets of the von Hippel-Lindau E3 ubiquitin ligase complex. *J Biol Chem*. 2003;278(13):11032–11040.
10. Hickey MM, Simon MC. Regulation of angiogenesis by hypoxia and hypoxia-inducible factors. *Curr Top Dev Biol*. 2006;76:217–257.
11. Gordan JD, Bertout JA, Hu CJ, Diehl JA, Simon MC. HIF-2alpha promotes hypoxic cell proliferation by enhancing c-myc transcriptional activity. *Cancer Cell*. 2007;11(4):335–347.
12. Bertout JA, et al. HIF2alpha inhibition promotes p53 pathway activity, tumor cell death, and radiation responses. *Proc Natl Acad Sci U S A*. 2009;106(34):14391–14396.
13. Takeda N, et al. Differential activation and antagonistic function of HIF-{alpha} isoforms in macrophages are essential for NO homeostasis. *Genes Dev*. 2010;24(5):491–501.
14. Bosch-Marce M, et al. Effects of aging and hypoxia-inducible factor-1 activity on angiogenic cell mobilization and recovery of perfusion after limb ischemia. *Circ Res*. 2007;101(12):1310–1318.
15. Sarkar K, Fox-Talbot K, Steenbergen C, Bosch-Marce M, Semenza GL. Adenoviral transfer of HIF-1alpha enhances vascular responses to critical limb ischemia in diabetic mice. *Proc Natl Acad Sci U S A*. 2009;106(44):18769–18774.
16. Tang N, et al. Loss of HIF-1alpha in endothelial cells disrupts a hypoxia-driven VEGF autocrine loop necessary for tumorigenesis. *Cancer Cell*. 2004;6(5):485–495.
17. Aragones J, et al. Deficiency or inhibition of oxygen sensor Phd1 induces hypoxia tolerance by reprogramming basal metabolism. *Nat Genet*. 2008;40(2):170–180.
18. Skuli N, et al. Endothelial deletion of hypoxia-inducible factor-2alpha (HIF-2alpha) alters vascular function and tumor angiogenesis. *Blood*. 2009;114(2):469–477.
19. Yamashita T, et al. Hypoxia-inducible transcription factor-2alpha in endothelial cells regulates tumor neovascularization through activation of ephrin A1. *J Biol Chem*. 2008;283(27):18926–18936.
20. Mazzone M, et al. Heterozygous deficiency of PHD2 restores tumor oxygenation and inhibits metastasis via endothelial normalization. *Cell*. 2009;136(5):839–851.
21. Noguera-Troise I, et al. Blockade of Dll4 inhibits tumour growth by promoting non-productive angiogenesis. *Nature*. 2006;444(7122):1032–1037.
22. Mesquita RC, et al. Hemodynamic and metabolic diffuse optical monitoring in a mouse model of hindlimb ischemia. *Biomed Opt Express*. 2010;1(4):1173–1187.
23. Gruber M, Hu CJ, Johnson RS, Brown EJ, Keith B, Simon MC. Acute postnatal ablation of Hif-2alpha results in anemia. *Proc Natl Acad Sci U S A*. 2007;104(7):2301–2306.
24. Ruzankina Y, et al. Deletion of the developmentally essential gene ATR in adult mice leads to age-related phenotypes and stem cell loss. *Cell Stem Cell*. 2007;1(1):113–126.
25. Ieronimakis N, Balasundaram G, Reyes M. Direct isolation, culture and transplant of mouse skeletal muscle derived endothelial cells with angiogenic potential. *PLoS One*. 2008; 3(3):e0001753.
26. Diez H, et al. Hypoxia-mediated activation of Dll4-Notch-Hey2 signaling in endothelial progenitor cells and adoption of arterial cell fate. *Exp Cell Res*. 2007;313(1):1–9.
27. Guidolin D, et al. Adrenomedullin stimulates angiogenic response in cultured human vascular endothelial cells: involvement of the vascular endothelial growth factor receptor 2. *Peptides*. 2008;29(11):2013–2023.
28. Yurugi-Kobayashi T, et al. Adrenomedullin/cyclic AMP pathway induces Notch activation and differentiation of arterial endothelial cells from vascular progenitors. *Arterioscler Thromb Vasc Biol*. 2006;26(9):1977–1984.
29. You LR, Lin FJ, Lee CT, DeMayo FJ, Tsai MJ, Tsai SY. Suppression of Notch signalling by the COUP-TFII transcription factor regulates vein identity. *Nature*. 2005;435(7038):98–104.
30. Tressel SL, et al. Angiopoietin-2 stimulates blood flow recovery after femoral artery occlusion by inducing inflammation and arteriogenesis. *Arterioscler Thromb Vasc Biol*. 2008;28(11):1989–1995.
31. Al Haj Zen A, Oikawa A, Bazan-Peregrino M, Meloni M, Emanueli C, Madeddu P. Inhibition of delta-like-4-mediated signaling impairs reparative angiogenesis after ischemia. *Circ Res*. 2010;107(2):283–293.
32. Cao L, Arany PR, Wang YS, Mooney DJ. Promoting angiogenesis via manipulation of VEGF responsiveness with notch signaling. *Biomaterials*. 2009;30(25):4085–4093.
33. Buas MF, Kadesch T. Regulation of skeletal myogenesis by Notch. *Exp Cell Res*. 2010;316(18):3028–3033.
34. Buas MF, Kabak S, Kadesch T. Inhibition of myogenesis by Notch: evidence for multiple pathways. *J Cell Physiol*. 2009;218(1):84–93.
35. Skuli N, Simon MC. HIF-1alpha versus HIF-2alpha in endothelial cells and vascular functions: is there a master in angiogenesis regulation? *Cell Cycle*. 2009;8(20):3252–3253.
36. Rey S, et al. Synergistic effect of HIF-1alpha gene therapy and HIF-1-activated bone marrow-derived angiogenic cells in a mouse model of limb ischemia. *Proc Natl Acad Sci U S A*. 2009;106(48):20399–20404.
37. Takeda Y, et al. Macrophage skewing by Phd2 haplodeficiency prevents ischaemia by inducing arteriogenesis. *Nature*. 2011;479(7371):122–126.
38. Yim SH, et al. Disruption of the Arnt gene in endothelial cells causes hepatic vascular defects and partial embryonic lethality in mice. *Hepatology*. 2006;44(3):550–560.
39. Werno C, et al. Knockout of HIF-1alpha in tumor-associated macrophages enhances M2 polarization and attenuates their pro-angiogenic responses. *Carcinogenesis*. 2010;31(10):1863–1872.
40. Imtiyaz HZ, et al. Hypoxia-inducible factor 2alpha regulates macrophage function in mouse models of acute and tumor inflammation. *J Clin Invest*. 2010;120(8):2699–2714.
41. Keith B, Johnson RS, Simon MC. HIF-1a and HIF-2a: sibling rivalry in hypoxic tumor growth and progression. *Nat Rev Cancer*. 2011;12(1):9–22.
42. Melillo G. Targeting hypoxia cell signaling for cancer therapy. *Cancer Metastasis Rev*. 2007;26(2):341–352.
43. Limbourg A, et al. Notch ligand Delta-like 1 is essential for postnatal arteriogenesis. *Circ Res*. 2007;100(3):363–371.
44. Thurston G, Noguera-Troise I, Yancopoulos GD. The Delta paradox: DLL4 blockade leads to more tumour vessels but less tumour growth. *Nat Rev Cancer*. 2007;7(5):327–331.
45. Kume T. Novel insights into the differential functions of Notch ligands in vascular formation. *J Angiogenes Res*. 2009;1:8.
46. Scott A, Fruttiger M. Oxygen-induced retinopathy: a model for vascular pathology in the retina. *Eye (Lond)*. 2010;24(3):416–421.
47. Chan CK, Pham LN, Zhou J, Spee C, Ryan SJ, Hinton DR. Differential expression of pro- and antiangiogenic factors in mouse strain-dependent hypoxia-induced retinal neovascularization. *Lab Invest*. 2005;85(6):721–733.
48. Jakobsson L, et al. Endothelial cells dynamically compete for the tip cell position during angiogenic sprouting. *Nat Cell Biol*. 2010;12(10):943–953.
49. Gustafsson MV, et al. Hypoxia requires notch signaling to maintain the undifferentiated cell state. *Dev Cell*. 2005;9(5):617–628.
50. Bertout JA, et al. Heterozygosity for hypoxia inducible factor 1alpha decreases the incidence of thymic lymphomas in a p53 mutant mouse model. *Cancer Res*. 2009;69(7):3213–3220.
51. Bedogni B, Warneke JA, Nickoloff BJ, Giaccia AJ, Powell MB. Notch1 is an effector of Akt and hypoxia in melanoma development. *J Clin Invest*. 2008;118(11):3660–3670.
52. Bryan L, Krock NS, Simon MC. Hypoxia-induced angiogenesis: good and evil [published online ahead of print September 27, 2011]. *Genes Cancer*. doi:10.1177/1947601911423654.
53. Selvin E, Erlinger TP. Prevalence of and risk factors for peripheral arterial disease in the United States: results from the National Health and Nutrition Examination Survey, 1999–2000. *Circulation*. 2004; 110(6):738–743.
54. Campa C, Harding SP. Anti-VEGF compounds in the treatment of neovascular age related macular degeneration. *Curr Drug Targets*. 2011;12(2):173–181.
55. Gotink KJ, Verheul HM. Anti-angiogenic tyrosine kinase inhibitors: what is their mechanism of action? *Angiogenesis*. 2010;13(1):1–14.
56. Alva JA, et al. VE-Cadherin-Cre-recombinase transgenic mouse: a tool for lineage analysis and gene deletion in endothelial cells. *Dev Dyn*. 2006;235(3):759–767.
57. Heil M, et al. Blood monocyte concentration is critical for enhancement of collateral artery growth. *Am J Physiol Heart Circ Physiol*. 2002; 283(6):H2411–H2419.
58. Niiyama H, Huang NF, Rollins MD, Cooke JP. Murine model of hindlimb ischemia. *J Vis Exp*. 2009;(23).pii:1035.
59. Winter SF, Acevedo VD, Gangula RD, Freeman KW, Spencer DM, Greenberg NM. Conditional activation of FGFR1 in the prostate epithelium induces angiogenesis with concomitant differential regulation of Ang-1 and Ang-2. *Oncogene*. 2007;26(34):4897–4907.
60. Limbourg A, Korff T, Napp LC, Schaper W, Drexler H, Limbourg FP. Evaluation of postnatal arteriogenesis and angiogenesis in a mouse model of hindlimb ischemia. *Nat Protoc*. 2009;4(12):1737–1746.
61. Marelli-Berg FM, Peek E, Lidington EA, Stauss HJ, Lechler RI. Isolation of endothelial cells from murine tissue. *J Immunol Methods*. 2000;244(1–2):205–215.